Journal of Medicinal Chemistry

Article

Development of novel quinoxaline-based kappa-opioid receptor (KOR) agonists for the treatment of neuroinflammation

Giovanni Tangherlini, Dmitrii V. Kalinin, Dirk Schepmann, Tao Che, nadine mykicki, Sonja Ständer, Karin Loser, and Bernhard Wünsch

J. Med. Chem., **Just Accepted Manuscript** • DOI: 10.1021/acs.jmedchem.8b01609 • Publication Date (Web): 13 Dec 2018

Just Accepted

ACS Publications

is published by the American Chemical Society. 1155 Sixteenth Street N.W., Washington, DC 20036

Development of novel quinoxaline-based κ-opioid receptor (KOR) agonists for the treatment of neuroinflammation

Giovanni Tangherlini,[a] Dmitrii V. Kalinin,[a] Dirk Schepmann,[a] Tao Che,[b] Nadine Mykicki,[c,d] Sonja Ständer,[c] Karin Loser,[c,d,e],Bernhard Wünsch* [a,e]

[a] Institut für Pharmazeutische und Medizinische Chemie der Universität Münster, Corrensstraße 48, D-48149 Münster, Germany.

Tel.: +49-251-8333311; Fax: +49-251-8332144; E-mail: wuensch@uni-muenster.de

[b] Department of Pharmacology, University of North Carolina at Chapel Hill, Chapel Hill, NC 27599, USA.

[c] Department of Dermatology, University of Münster, von-Esmarch-Str. 58, D-48149 Münster, Germany

[d] CRC1009 *Breaking Barriers* and CRC-TR 128 *Multiple Sclerosis*, University of Münster, Germany

[e] Cells-in-Motion Cluster of Excellence (EXC 1003 – CiM), Westfälische Wilhelms-Universität Münster, D-48149 Münster, Germany.

Abstract

Neuroinflammatory disorders, such as multiple sclerosis (MS) or experimental autoimmune encephalomyelitis (EAE), an established mouse model mimicking part of the human pathology, are characterized by inflammatory infiltrates containing T helper 1 (T_H1) and T_H17 cells, which cause demyelination and neurodegeneration. Disease onset

and perpetuation are mediated by peripherally generated autoreactiveT cells infiltrating into the central nervous system, where they are re-stimulated by antigen-presenting cells. Here, we show that newly designed peripherally active, potent and selective κ-opioid receptor (KOR) agonists comprising the ethylenediamine KOR pharmacophore in a perhydroquinoxaline scaffold exhibit potent anti-inflammatory capacities in primary antigen presenting cells as well as T cells. In the EAE model the secondary amine **12** and the triazole **14** were able to ameliorate disease severity and to delay disease onset by blocking effector T cell activation. Importantly, the beneficial effects were mediated via signaling through KOR since off-target effects were excluded by using KOR deficient mouse mutants.

Key words

KOR agonists; perhydroquinoxaline; selectivity; agonistic activity; structure-activity relationships; docking; anti-inflammatory activity; T_H1 or T_H17 effector cells; experimental autoimmune encephalomyelitis; KOR deficient mouse mitants

1. Introduction

Multiple sclerosis (MS) is one of the most common chronic, autoimmune, inflammatory and demyelinating disorders of the central nervous system (CNS) affecting 2.5 million people worldwide with a high incidence in young adults.[1-3] MS is considered a T-cell-mediated disease, where peripherally generated autoreactive T cells producing interferone-γ (IFN-γ) or interleukin-17 (IL17) are supposed to infiltrate into the CNS and

to be responsible for the initiation of the disease.[2] After entering the CNS, these T cells are restimulated by antigen-presenting cells resulting in local expansion of pathogenic T helper 1 (T_H1) and T_H17 cells, tissue damage to oligodendrocytes, and a subsequent infiltration of bystander immune cells, controlling disease perpetuation.[3] In experimental autoimmune encephalomyelitis (EAE), a mouse model mimicking part of the human MS pathology, the lung has been identified as a niche, where pathogenic T cells are stimulated, proliferate and acquire migratory properties to enter the CNS. Thus, peripheral organs seem to contribute to the activation of CNS-reactive T cells and their transition into a migratory state.[4] In MS as well as in EAE regulatory T cells (Treg) have been shown to be involved in limiting the proliferation and infiltration of pathogenic T_H1 and T_H17 cells into the CNS.[5] However, a modified phenotype and an impaired suppressive activity of Treg has been associated with disease progression.[6–8]

Since MS lesions can be detected in different parts of the brain, a big variety of symptoms are observed in patients, such as sensory or motor disturbances, acute or chronic pain, depression and optic neuritis.[2,9]

Since the launch of the first drug against MS in 1993, several immunomodulatory treatments were developed.[10] Interferon-β-1b (IFN-β),[11] glatiramer acetate (GLAT),[12] DNA intercalating drugs such as mitoxantrone,[13] spingosine-1-phosphate (S1P) receptor antagonists, such as fingolimod,[14] and dimethyl fumarate[15] finally induce anti-inflammatory pathways via different mechanisms of action. Additionally, various monoclonal antibodies,[16,17] including natalizumab and ocrelizumab, are able to inhibit the infiltration of immune cells into the CNS. All these drugs have been shown to reduce the

relapse rate and to improve the disability in relapsing-remitting MS.[18] However, they are not able to stop disease perpetuation.[2] In addition, all drugs currently used for MS treatment can have adverse effects ranging from mild, such as flu-like symptoms or irritations at the injection site, to serious, like progressive multifocal leukoencephalopathy (PML), a viral disease of the CNS.[19] For this reason, novel drugs addressing new mechanisms of action are urgently needed.

Recent studies suggested the endogenous opioid system to play a special role in the pathogenesis of MS inflammatory neurodegeneration.[20–22] The effects of this system are predominantly mediated by three G-protein-coupled receptors, called μ- (MOR), δ- (DOR) and κ-opioid receptor (KOR).[23] They are present in the CNS but also in peripheral tissues and cells, such as skin, intestine and immune cells, including T cells and antigen presenting cells.[23,24] The opioid system is commonly associated with pain transmission and with different psychiatric disorders, such as depression, anxiety and addiction.[23,25]

During the last years, KOR acquired increasing attention in research and emerged as an alternative target for the development of safer analgesics.[26,27] In particular, KOR activation results in strong analgesia, but does not lead to typical MOR-mediated side effects, such as euphoria, respiratory depression and dependelnce.[26,27] In 2009, the selective KOR agonist nalfurafine was approved in Japan for the treatment of uremic pruritus.[28] Clinical studies showed that KOR partial agonists or antagonists, such as buprenorphine and CERC-501, are promising drugs for the treatment of major depression and abuse disorders.[25,27,29] A few recent studies suggest a potential role of KOR in inflammatory neurodegeneration. Screening of mRNA in Theiler's murine

encephalomyelitis, a virus model mimicking part of the MS pathology showed a decreased level of KOR mRNA.[21] Additionally, KOR has the ability to down-regulate the proliferation, activation and secretion of cytokines in immune cells pointing to its antiinflammatory activity.[30] Furthermore, very recent data in EAE showed the ability of activated KOR to prevent neuronal damage and to promote remyelination. Moreover, ligation of KOR by a selective agonist seems to be involved in the differentiation of oligodendrocyte progenitor cells (OPC) towards myelinated oligodendrocytes.[20] Due to their ability to regulate cytokine production and immune cell activation, KOR agonists may represent a novel promising approach for the treatment of neuroinflammatory or neurodegenerative disorders such as MS or EAE.[20]

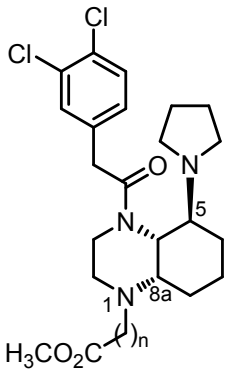

n = 0: (4a*R*,5*S*,8a*S*)-**1a**
n = 1: (4a*R*,5*S*,8a*S*)-**1b**

Figure 1: KOR agonists (4a*R*,5*S*,8a*S*)-**1a**,**b** with *cis*-configuration of the annulated ring system and *trans*-orientation of the pyrrolidine ring.

Recently, we have reported that perhydroquinoxalines (4a*R*,5*S,*8a*S*)-**1a**,**b** (Figure 1) represent potent and selective KOR agonists (K_i(**1a**) = 0.25 nM, EC_{50} = 2.0 nM, (K_i(**1b**) = 0.70 nM). The *cis*-configuration of the annulated rings and the relative *trans*-orientation

of the pyrrolidine ring are crucial for high KOR affinity and agonistic activity.[31,32] In the arachidonic acid-induced ear inflammation model, enantiomerically pure quinoxaline (4a*R*,5*S,*8a*S*)-**1a** and some analogous KOR agonists showed anti-inflammatory activity comparable to those of indomethacin or hydrocortisone.[33]

With the aim to contribute to potential further clinical development towards novel MS therapeutics, a further improvement of quinoxaline-based KOR agonists of type **1** was envisaged. In particular, the polarity of the ligands should be increased by introduction of a second basic amino moiety (4-position) or a polar triazole ring within the substituent in 4-position. Moreover, the interaction with KOR, the anti-inflammatory effect on primary mouse and human immune cells as well as the *in vivo* efficacy of the new KOR agonists in EAE were investigated.

2. Result and discussion

2.1. Synthesis

In order to get fast access to perhydroquinoxaline derivatives with various substituents in 1-position (Figure 1) the strategy of late-stage diversification was pursued. For this purpose the secondary amine **12** was selected as building block, which allows the introduction of diverse substituents in 1-position. (Scheme 1)

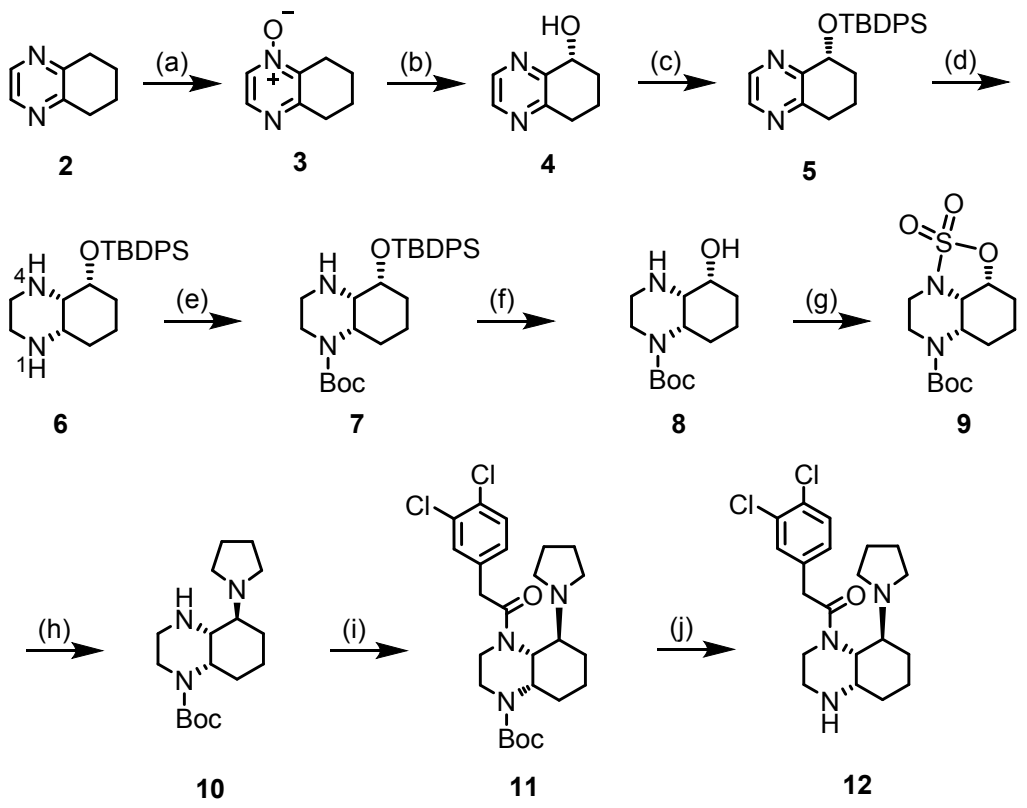

Scheme 1: Synthesis of central building block **12**.

Reagents and conditions: (a) *m*-CPBA, CH_2Cl_2, rt, 22 h, 89 %; (b) 1: acetic anhydride, 120 °C, 5 h; 2: aq. NaOH 4 M, CH_3OH, rt, 12 h, 71 %; (c) TBDPSCl, imidazole, 4-DMAP, CH_2Cl_2, rt, 16 h, 98 %; (d) H_2 (5 bar), PtO_2, CH_3OH, AcOH, rt, 5 h, 88 %; (e) Boc_2O, CH_2Cl_2, rt, 18 h, 87 %; (f) TBAF, THF, rt, 4 h, 73 %; (g) 1: $SOCl_2$, imidazole, CH_2Cl_2, -78 °C, 17 h; 2: $NaIO_4$, $RuCl_3.H_2O$, CH_3CN/EtOAc 6:1, 0 °C, 12 h, 88 %; (h) pyrrolidine, CH_3CN, 80 °C, 16 h, 72 %; (i) 2-(3,4-dichlorophenyl)acetyl chloride, CH_2Cl_2, 0 °C, 2-5 h, 84 %; (j) CF_3CO_2H, CH_2Cl_2, rt, 16 h, 98 %.

Only one enantiomer of the racemic mixtures is shown.

In order to obtain higher yields and adapt the conditions to our research laboratory, the originally reported industrial synthesis of compounds **1**[32,33] was modified. In Scheme 1

the modified synthesis starting with tetrahydroquinoxaline (**2**) is displayed. At first, the N-oxide **3** was prepared by oxidation of quinoxaline **2** with m-CPBA. The subsequent *Boekelheide* rearrangement[34] of N-oxide **3** was performed with Ac_2O instead of trifluoroacetic anhydride which gave higher yields of benzylic alcohol **4** after hydrolysis with NaOH and methanol. The hydroxy moiety of **4** was then protected by a silyl group. Instead of the *tert*-butyldimethylsilyl protective group[33] the *tert*-butyldiphenylsilyl (TBDPS)[35] protective group was chosen for four main reasons: (1) the very large TBDPSO group should direct the hydrogenation from the opposite site leading to *cis,cis*-configured perhydroquinoxaline **6** with high diastereoselectivity; (2) the large TBDPSO group should shield the adjacent NH-group of product **6** in order to achieve high regioselectivity during the Boc-protection; (3) the TBDPSO-group should be stable under the harsh conditions during hydrogenation, which requires a pressure of 5 bar H_2 and the addition of HOAc to the methanolic solution; (4) The UV-absorption of the phenyl rings allows an easy detection of educts and products by TLC and HPLC.

As expected, hydrogenation (H_2, 5 bar, PtO_2, CH_3OH, HOAc) of the TBDPS-protected tetrahydroquinoxalinol **5** led exclusively to the *cis,cis*-configured perhydroquinoxaline **6** in 88 % yield. This transformation represents the key step of the overall diastereoselective synthesis, since only one diastereomer (*cis,cis*) of four theoretically possible diastereomers was formed by the backside attack of H_2 at the aromatic pyrazine ring.

Next, perhydroquinoxaline **6** was reacted with $(Boc)_2O$ to afford the mono-Boc-protected quinoxaline **7**. The large TBDPSO group inhibits the acylation of the NH moiety in 4-position resulting in exclusive formation of **7**. After having fulfilled its task, the TBDPS-

protective group of **7** was removed with tetrabutylamonium fluoride (TBAF) to provide the β-amino alcohol **8**.

According to literature, β-amino alcohol **8** was converted into the cyclic sulfuric acid ester amide **9** using SO_2Cl_2. In our hands a two-step procedure[36] involving the reaction of β-amino alcohol **8** with $SOCl_2$ and subsequent oxidation with $NaIO_4$ and $RuCl_3$ gave higher yields (88 %) of the desired 1,2,3-oxathiazolidine **9**. It has to be noted that the NMR spectra of the intermediate after reaction of **8** with $SOCl_2$ is rather complex, since the S-atom represents an additional center of chirality. After oxidation, clear signals in the NMR spectra confirm the structure of the cyclic sulfuric acid derivative **9**. The cyclic sulfuric acid derivative fulfills two tasks. First of all, it protects the secondary amino moiety in 4-position. Secondly, it transformed the OH moiety in 5-position into a good leaving group suitable for S_N2 substitution.

The nucleophilic substitution of **9** with pyrrolidine was the second key step in the synthetic route. The transformation proceeded as pure S_N2 reaction with inversion of configuration at C-5 affording the desired *cis,trans* configuration in quinoxaline **10**.[33] After acylation of the free secondary amine **10** with 2-(3,4-dichlorophenyl)acetyl chloride (**11**), the Boc protective group was cleaved off using trifluoroacetic acid in order to isolate the secondary amine **12** as promising building block in 98 % yield.

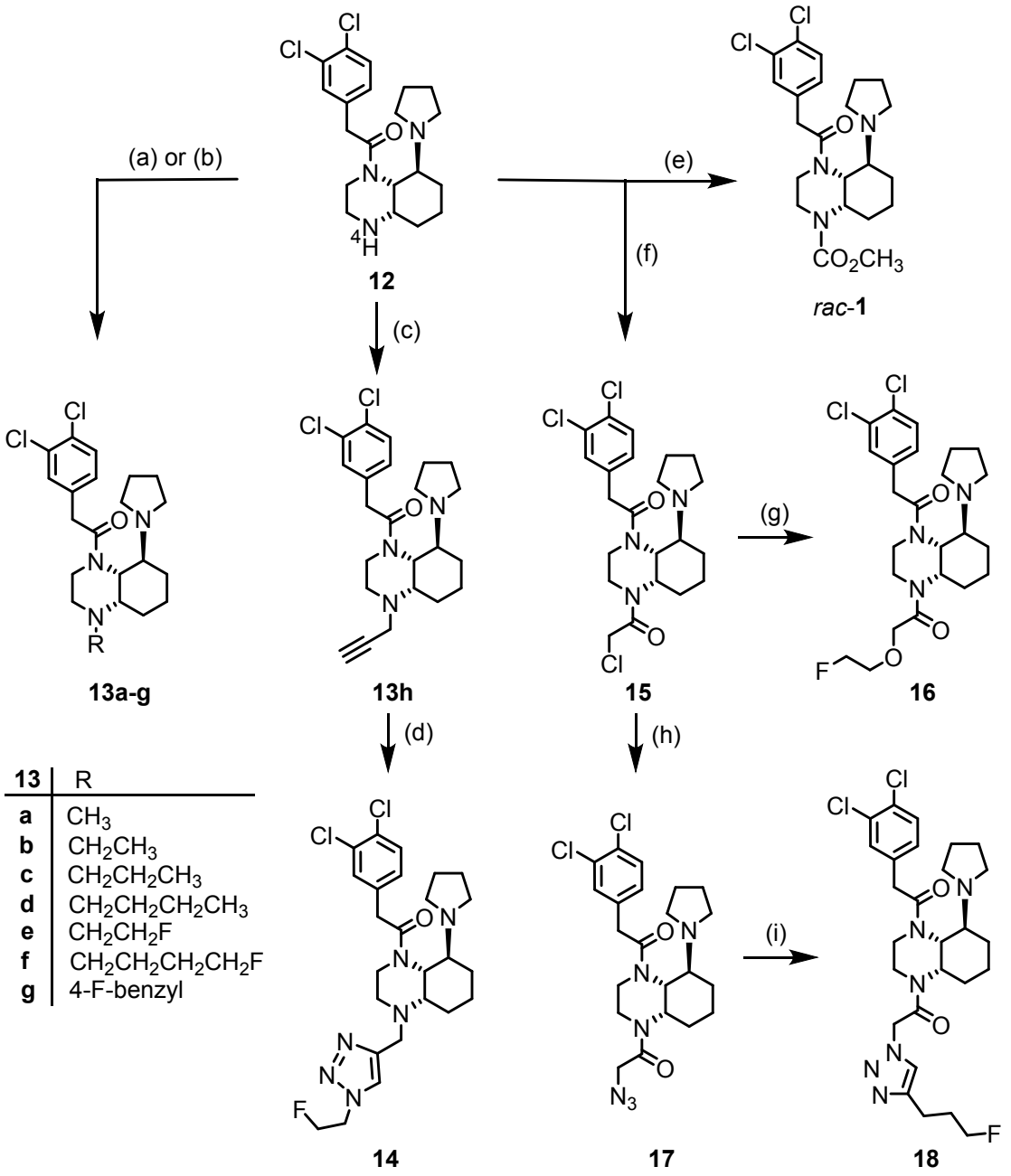

Scheme 2: Late stage diversification of building block secondary amine **12**.

Reagents and conditions: (a) RCH=O, $NaBH_3CN$, CH_3CO_2H, CH_3OH, rt, 16 h, 54 % (**13a**), 69 % (**13b**), 66 % (**13c**), 85 % (**13d**), 42 % (**13g**). (b) RCH=O, $NaBH(OAc)_3$, CH_2Cl_2, 0 °C, 17 h, 65 % (**13e**), 51 % (**13f**); (c) propargyl bromide, Cs_2CO_3, DMF, 40 °C, 16 h, 92 %; (d) 2-fluoroethyl azide, $CuSO_4$, sodium ascorbate, DMF/H_2O, rt, 4 h, 35 %; (e) methyl chloroformate, pyridine, CH_2Cl_2, 0 °C, 1 h, 98 %; (f) 2-chloroacetyl chloride, Et_3N, CH_2Cl_2,

0 °C, 5 h, 73 %; (g) 2-fluoroethanol, NaH, THF, 0 °C, 40 h, 39 %; (h) NaN_3, DMF, rt, 20 h, 91 %; (i) 5-fluoropent-1-yne, $CuSO_4$, sodium ascorbate, DMF/H_2O, rt, 3 h, 17 %. Only one enantiomer of the racemic mixtures is shown.

Scheme 2 shows the formation of diverse test compounds using the common building block **12**. Quinoxaline derivatives **13a**-**g** bearing various alkyl side chains in 4-position were obtained by reductive alkylation of secondary amine **12** with various aldehydes and $NaBH_3CN$ or $NaBH(OAc)_3$. Since alkylation of **12** with fluoroalkyl halides failed to give **13e** and **13f**, fluoroacetaldehyde and 4-fluorobutyraldehyde were prepared in situ by oxidation of the corresponding alcohols with Dess-Martin-Periodinane and the crude aldehydes were directly used in the reductive alkylation reaction.[31,37] The fluorobenzyl derivative **13g** was synthesized to investigate the effect of a large and more lipophilic fluorobenzyl moiety on the interaction with KOR.

The propargyl derivative **13h** was obtained by alkylation of secondary amine **12** with propargyl bromide. Cu^+-catalyzed 1,3-dipolar cycloaddition[38,39] of alkyne **13h** with 2-fluoroethyl azide provided the triazole derivative **14**. The triazole moiety led to increased size and polarity of the side chain. The increased polarity is of particular importance, since we are interested in KOR agonists which are not able to pass the blood-brain-barrier.

Acylated quinoxalines **1** and **15** were obtained by acylation of secondary amine **12** with methyl chloroformate and 2-chloroacetyl chloride, respectively. The racemic methyl carbamate **1** was prepared for comparison of its KOR affinity and activity with those of the newly synthesized KOR ligands. Reaction of the chloroacetamide **15** with 2-

fluoroethanol and NaH[40] afforded the fluoroethyl ether **16** in 80 % yield. Nucleophilic substitution of **15** with NaN_3 led to the azide **17**, which underwent a 1,3-dipolar cycloaddition (click reaction)[38,41] with 5-fluoropent-1-yne to produce fluoropropyltriazole **18**.

2.2. Pharmacological evaluation

KOR affinity

The KOR affinity of the synthesized quinoxaline derivatives and some reference compounds was investigated in competitive radioligand binding assays using guinea pig brain homogenates as source of KOR and [^{3}H]U-69,593 as competitive radioligand. The data in Table 1 summarize the KOR affinity of the test compounds.[42–44]

Table 1: Affinities of perhydroquinoxalines and reference compounds towards KOR and related receptors.

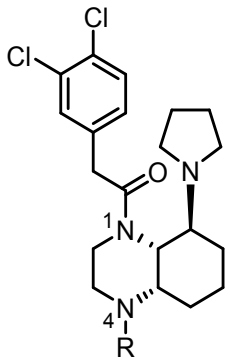

compd.	R	K_i ± SEM [nM] [a) b)]				
		KOR	MOR	DOR	σ_1	σ_2
		[^{3}H]U-69,593	[^{3}H]DAMGO	[^{3}H]DPDPE	[^{3}H]-(+)-pentazocine	[^{3}H]DTG
rac-**1a**	CO_2CH_3	1.3 ± 0.4	0 %	250	0 %	8 %

11	$CO_2C(CH_3)_3$	3.8 ± 1.2	260	438	12 %	16 %
12	H	0.54 ± 0.15	28 %	205	0 %	5 %
13a	CH_3	2.3 ± 1.3	0 %	333	0 %	4 %
13b	CH_2CH_3	4.2 ± 1.7	3300	1100	11 %	16 %
13c	$CH_2CH_2CH_3$	1.4 ± 0.2	407	992	1800	2400
13d	$CH_2CH_2CH_2CH_3$	6.6 ± 3.1	2600	2500	876	1300
13e	CH_2CH_2F	2.2. ± 0.2	12 %	5 %	12 %	3 %
13f	$CH_2CH_2CH_2CH_2F$	8.0 ± 3.0	8 %	17 %	0 %	8 %
13g	4-F-Bn	81 ± 21	0 %	397	1600	0 %
14	CH_2-triazole-CH_2CH_2F	5.6 ± 0.6	573	413	2 %	0 %
16	$C(=O)CH_2OCH_2CH_2F$	15 ± 3	0 %	1100	13 %	0 %
18	$C(=O)CH_2$-triazole-$CH_2CH_2CH_2F$	3.3 ± 1.3	947	425	0 %	0 %
U-69,593		0.97 ± 0.40	-	-	-	-
naloxone		7.3 ± 0.40	2.3 ± 1.1	103	-	-
morphine		-	5.2 ± 1.6	-	-	-
SNC80		-	-	1.2 ± 0.5	-	-
(+)-pentazocine		-	-	-	5.4 ± 0.5	-
haloperidol		-	-	-	6.6 ± 0.9	78 ± 2.3

[a] A value in % reflects the inhibition of the radioligand binding at a test compound concentration of 1 µM. K_i values without SEM values represent the mean of two experiments (n = 2) and K_i values with SEM values represent the mean of three experiments (n = 3).

[b] Guinea pig brain membrane preparations were used in the KOR, MOR and σ_1 assay. In the DOR assay rat brain and in the σ_2 assay rat liver membrane preparations were used.

With exception of the 4-fluorobenzyl derivative **13g** and the fluoroethoxy derivative **16** the K_i values reflecting KOR affinity of all new test compounds are lower than 10 nM indicating very high KOR affinity. The length of the side chain of the N-4 substituent seems not to play a crucial role for the interaction with KOR, as the quinoxalines **13a**-**13d** with homologous alkyl substituents display almost the same KOR affinity. Even the quinoxaline **11** with the large and bulky *tert*-butoxycarbonyl moiety shows high KOR affinity (K_i = 3.8 nM). It is postulated that the N-4-substituent is oriented towards the entrance channel and the surface of KOR. This hypothesis is supported by the triazole derivatives **14** and **18** showing KOR affinity of 5.6 nM and 3.3 nM, respectively. Hydrophilic interactions of surrounding water molecules with the polar triazole rings within the large N-4-substituents may explain the high KOR affinity of **14** and **18**.

Moreover, KOR accepts both alkyl and acyl moieties at N-4. Although the basicity and the geometry of differently substituted derivatives are quite diverse, the KOR affinity of pairs with analogous alkyl and acyl moieties are quite similar. As an example, the KOR affinity of **13c** with a propyl moiety at N-4 is 1.4 nM and the KOR affinity of the methoxycarbonyl

derivative **1** is 1.3 nM. This observation supports the hypothesis that the binding pocket of KOR accepts substituents with different size at N-4. Furthermore, a second basic amino group (N-4) in the ligand is also well accepted by KOR.

Since a fluorinated PET tracer for selective labeling of KORs represents a long term aim in our group, fluorine atoms were introduced at different positions. In general, high KOR affinity was found for quinoxalines with a F-atom at the N-4 alkyl side chain (e.g. **13e**, **13f**) or at the triazole side chain (**14**, **118**).

*Interactions of **14** with KOR (docking)*

To rationalize the observed KOR affinity of triazole **14**, the compound was docked into the crystal structure of KOR in its active state (PDB: 6B73[66]). The obtained docking pose of **14** (Figure 2) is consistent with previously reported docking modes of its conformationally unrestricted analogues U50,488 and U69,593.[66] Thus, protonated tertiary amino moiety of the pyrrolidine ring of **14** forms an ionic interaction with Asp138, whereas the O-atom of the carbonyl moiety forms an H-bond with Gln115. The pyrrolidine ring is additionally involved in the lipophilic contacts with a number of amino acid residues *e.g.* Met142, Tyr320, Trp287, and Asp138. The perhydroquinoxaline scaffold of **14** from one side of the pocket forms hydrophobic contacts with Ile290, Ile294, and Trp287, and from the other side with Tyr139. The dichlorophenyl moiety of **14** occupies a hydrophobic site of the pocket undergoing lipophilic interactions with Leu135 and Gln115. Finally, the triazole ring of **14** forms nonpolar interactions with Lys227 and Tyr139 pointing fluoroethyl moiety toward the extracellular region of the receptor.

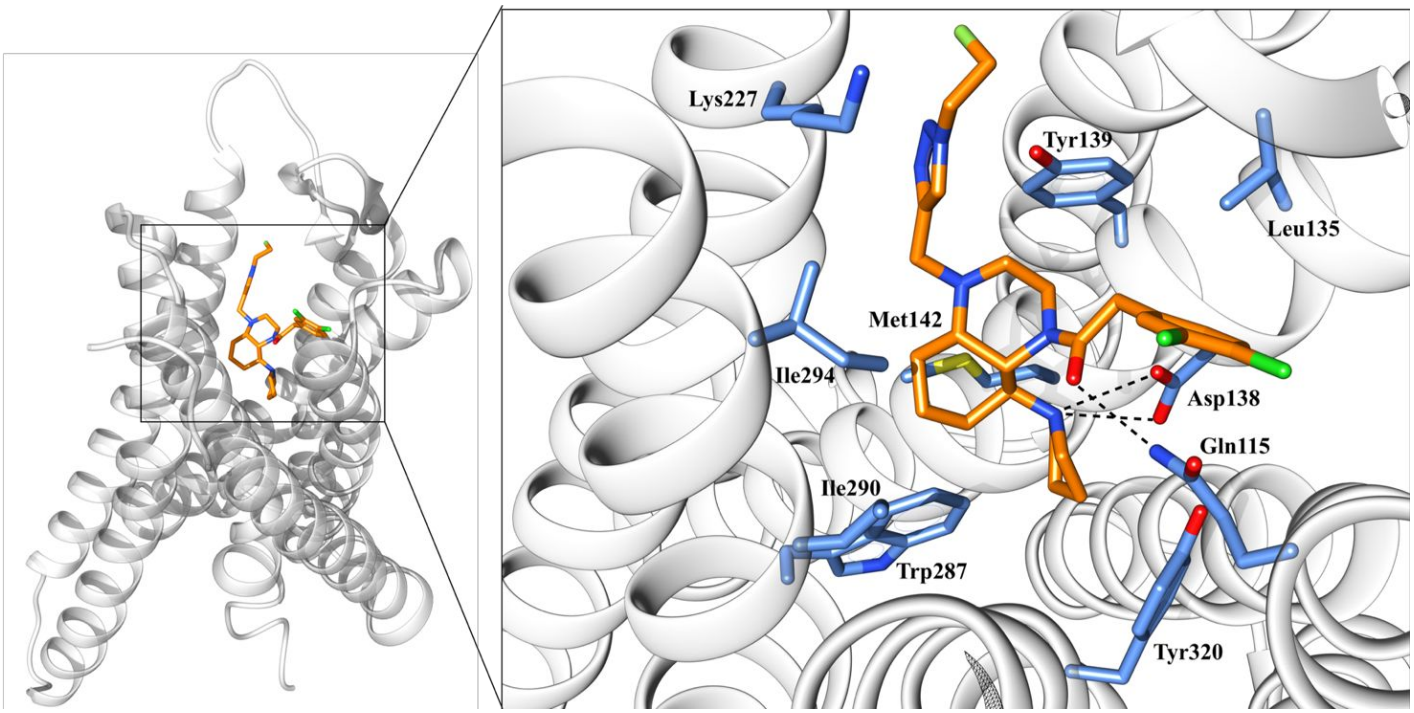

Figure 2: Binding mode (docking pose) of compound **14** (orange stick model) in the active state of KOR (PDB: 6B73[66]). Amino acid residues are depicted as blue stick models. Oxygen, nitrogen, sulfur, fluorine, and chlorine atoms are colored in red, blue, yellow, light green, and green, respectively. Hydrogen bonds are depicted as dashed lines (black).

Selectivity over MOR, DOR and σ receptors

In order to analyze the selectivity of the potent KOR agonists, competitive radioligand binding studies were performed to determine MOR, DOR, σ_1 and σ_2 affinity of the ligands. In the MOR and DOR assay, receptor preparations from rat brain and the radioligands [^{3}H]DAMGO and [^{3}H]DPDPE were employed, respectively. σ_1 and σ_2 receptor affinity were recorded using guinea pig brain and rat liver membrane preparations and [^{3}H](+)-pentazocine and [^{3}H]di-*o*-tolylguanidine as radioligands, respectively.[64,65] At first quinoxalines were tested at a concentration of 1 μM. The complete competition curves

were recorded only when the binding of the radioligand was reduced by more than 50 %. Otherwise, the inhibition of radioligand binding (in %) at a test compound concentration of 1 μM is given in Table 1.

The quinoxaline derivatives show very low affinity towards MOR and DOR (K_i > 200 nM) resulting in high KOR:MOR and KOR:DOR selectivity. (Table 1) Extraordinarily high selectivity was recorded for quinoxalines with particular relevance for this project, i.e. secondary amine **12** (KOR:MOR > 1800, KOR:DOR = 380), fluoroethyl derivative **13e** (KOR:MOR > 4500, KOR:DOR > 450), fluoroethyltriazole **14** (KOR:MOR = 100, KOR:DOR = 74) and fluoropropyltriazole **18** (KOR:MOR > 285, KOR:DOR = 130).

It has been reported that small modifications of KOR agonists led to high σ receptor affinity. For example, the change of the *trans*-configured prototypical KOR agonist U-50,488, to its *cis*-configured analog generated a ligand with high σ receptor affinity.[45] Moreover, reduction of the phenylacetamide moiety of monoacylated ethylenediamine KOR agonists to a phenylethylamino group further increased the σ affinity and decreased the KOR affinity.[46] For this reason, σ_1 and σ_2 affinity of the novel KOR agonists were also recorded. (Table 1) The data in Table 1 clearly demonstrate that the quinoxaline-based KOR agonists do not substantially interact with σ_1 and σ_2 receptors. The highest σ_1 and σ_2 affinities were found for the butyl derivative **13d** ($K_i(\sigma_1)$ = 876 nM, $K_i(\sigma_2)$ = 1300 nM). Nevertheless, the KOR:σ_1 and KOR:σ_2 selectivity of **13d** is 135 and 230, respectively. The extraordinarily high KOR:σ_1 and KOR:σ_2 selectivity of the important quinoxalines **12**, **13e**, **14** and **18** of greater than 180 should be emphasized here.

In conclusion, the newly synthesized KOR agonists show high selectivity against MOR, DOR, σ_1 and σ_2 receptors.

Functional activity

In order to further explore the pharmacological potential of quinoxaline-based KOR agonists, the KOR affinity of the most promising ligands was investigated in a second binding assay. In this assay, the human KOR was transiently expressed in HEK 293T cells and [^{3}H]diprenorphine was used as radioligand.[47] Table 2 correlates the affinity data obtained with human and guinea pig KORs.

Table 2: Activity of selected KOR agonists correlated with KOR affinity.

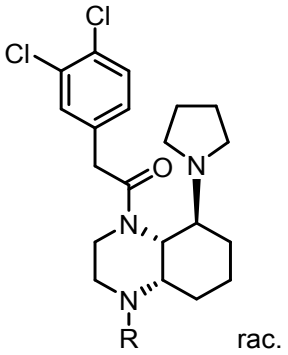

rac.

compd.	R	K_i ± SEM [nM]		cAMP[b]		β-arrestin-2[c]	
		KOR[a]	KOR[b]				
		[^{3}H]U-69,593	[^{3}H]diprenor-phine	*EC*$_{50}$ ± SEM [nM]	E_{max}± SEM %[d]	EC_{50} ± SEM [nM]	E_{max}± SEM %[d]
11	$CO_2C(CH_3)_3$	3.8 ± 1.2	18 ± 1.2	8.1 ± 0.8	94 ± 2	42 ± 1.2	102 ± 4
12	H	0.54 ± 0.15	4.8 ± 0.9	1.2 ± 0.4	103 ± 2	3.8 ± 0.8	93 ± 1
13a	CH_3	2.3 ± 1.3	11 ± 1.0	3.4 ± 0.5	102 ± 2	17 ± 0.7	101 ± 2
13b	CH_2CH_3	4.2 ± 1.7	11 ± 0.5	2.0 ± 0.4	103 ± 2	12 ± 0.6	99 ± 3
13c	$CH_2CH_2CH_3$	1.4 ± 0.2	9.2 ± 0.8	1.6 ± 0.3	102 ± 1	7.9 ± 0.9	108 ± 4

13d	$CH_2CH_2CH_2CH_3$	6.6 ± 3.1	16 ± 1.3	6.0 ± 0.8	102 ± 3	33 ± 1.3	106 ± 5
13g	4-F-Bn	81 ± 21	42 ± 2.6	32 ± 1.8	97 ± 3	247 ± 4.2	105 ± 5
14	CH_2-triazole-CH_2CH_2F	5.6 ± 0.6	46 ± 2.1	2.8 ± 0.2	103 ± 1	43 ± 1.4	86 ± 3
16	$C(=O)CH_2OCH_2CH_2F$	15 ± 3	77 ± 4.7	10 ± 0.6	97 ± 2	227 ± 3.8	103 ± 4
U-69,593		0.97 ± 0.40	-	-		-	
Diprenorphine			0.69 ± 0.08	-		-	
salvinorin A		-	-	0.015		5.1	

a) Guinea pig brain membrane preparations.

b) Human HEK 293T cells.

c) Human HTLA cells.

d) The E_{max} values refer to salvinorin A (100 %).

With exception of the fluorobenzyl derivative **13g**, the K_i values obtained at human KORs (transfected HEK-293T cells) are generally 3-9-fold higher than the K_i values recorded with guinea pig brain preparations. This is due to the different properties of the radioligands used in the binding assays. While [^{3}H]U69,593 at 1 nM labels only the high-affinity sites and thus $K_{observed}$ is the K_{high}, [^{3}H]diprenorphine at 1.5 nM could label both high- and low-affinity sites, so $K_{observed}$ is the average of both. This is also supported by the same tendencies observed in both assay systems, e.g. the tertiary amines **13a** and **13b** have K_i values of 11 and 11 nM at the human KOR and K_i values of 2.3 and 4.2 nM at the guinea pig KOR.

In order to detect potency and efficacy in KOR-mediated signaling pathways, the functional activity of the quinoxaline-based KOR agonists was recorded in a cAMP inhibition assay and a Tango β-arrestin-2 recruitment assay.[67,68]

In Table 2 the EC_{50}-values of the quinoxaline-based KOR agonists are displayed and compared with the EC_{50}-values of reference compound salvinorin A. The quinoxaline analogs are all full agonists at KOR. The tested compounds show remarkably high activation of the G_i-dependent pathway with EC_{50} values below 10 nM. As expected from the low KOR affinity, the fluorobenzyl derivative **13g** has rather low agonistic activity (EC_{50} = 32 nM). Regarding the β-arrestin-2 recruitment, most of the tested quinoxalines show slightly lower β-arrestin-2 activation than salvinorin A.

The very high KOR activation of the secondary amine **12** with EC_{50}-values of 1.2 nM and 4.8 nM in the cAMP and β-arrestin-2 recruitment assay, respectively, should be emphasized. In addition to **12**, the fluoroethyltriazole **14** shows also high KOR affinity and KOR agonistic activity in the cAMP assay. The calculated clogP values for **12** (clogP = 3.70) and **14** (clogP = 3.80) are in the same ragne as the clogP value of **1b** (clogP = 3.81). As **1b** did not show any central effects in vivo,[33] low CNS penetration of **12** and **14** was expected.

Anti-inflammatory activity of the quinoxaline-based KOR agonists in vitro

Several studies revealed that β-arrestins are functionally involved in inflammation and autoimmunity. Accordingly, mice deficient for β-arrestin-2 showed exacerbated symptoms of EAE, which. was mediated by decreased numbers of $Foxp3^+$ regulatory T cells, a cell subset, which usually controls the activation and expansion of pathogenic T_H1 or T_H17 effector cells .[48] Also cAMP has been associated with EAE perpetuation. In addition to a direct impact of the cAMP pathway on $CD4^+$ T cells by inhibiting the proliferation and IFN-γ secretion in encephalitogenic T cells, stimulation of the cAMP pathway polarized macrophages towards an M2-like phenotype, leading to indirect inhibition of effector T cell activation.[49] Based on these observations and since we already identified decahydroquinoxaline KOR agonists with a strong anti-inflammatory potential,[33] we intended to characterize the effect of the secondary amine **12** and the fluoroethyltriazole derivative **14** on immune cells involved in the perpetuation of neuroinflammation and to assess the therapeutic potential of both compounds in EAE.

Therefore, we first investigated the anti-inflammatory properties of compounds **12** and **14** on T cells and dendritic cells (DC), which were purified from peripheral blood of healthy human donors or secondary lymphatic organs of mice. The cells were stimulated with phorbol 12-myristate 13-acetate (PMA) in combination with ionomycin (PMA/Iono) to up-regulate the expression of typical activation markers and the secretion of pro-inflammatory cytokines. In MS as well as in EAE naive T cells differentiate into effector cells in the peripheral immune system by direct contact to mature DC that express co-stimulatory receptors such as CD40, CD80 or CD86 and secrete pro-inflammatory cytokines including IFN-γ, IL-12, IL-23 or IL-6.[50,51] These effector T cells are able to cross

the blood-brain barrier (BBB), migrate into the CNS and promote demyelination, axonal damage and finally, the formation of inflammatory foci.[50] MS and EAE have long been considered as T cell-mediated diseases and it has been shown that particularly T_H1 and T_H17 cells secreting INF-γ and IL-17 are markedly increased in cerebrospinal fluid (CSF) from MS patients and in CNS tissue from EAE mice.[51–54]

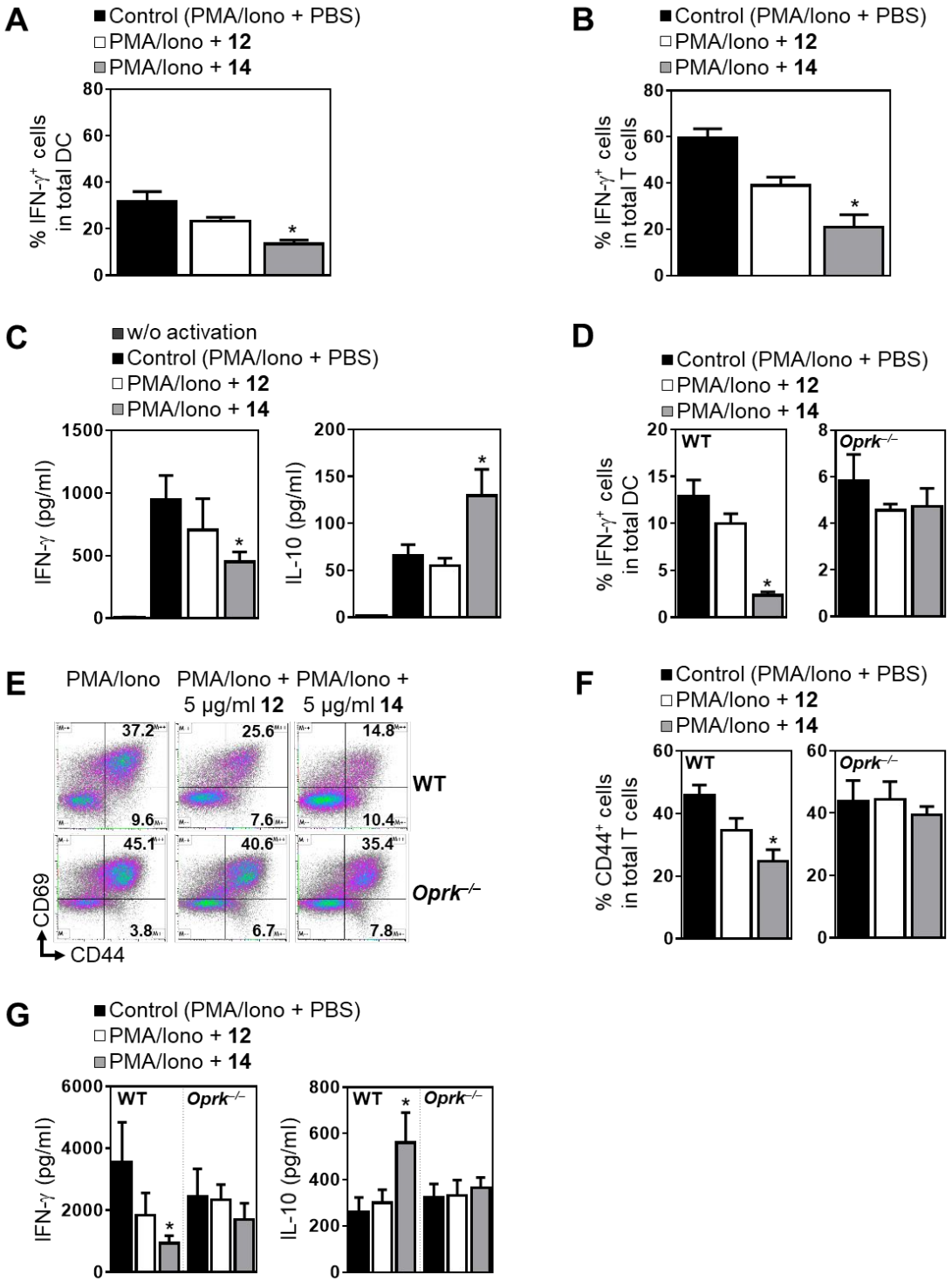

Figure 3: Fluoroethyltriazole **14** significantly reduced the expression of pro-inflammatory cytokines in human and mouse immune cells via binding to KOR. (**A**, **B**) DC (**A**) and T cells (**B**) were sorted from human peripheral blood mononuclear cells (PBMC) by

magnetic beads and activated with PMA + ionomycin (PMA/Iono) for 12 h as described. Subsequently, cells were stimulated with compounds **12** or **14** (5 µg/mL each) for additional 48 h. Control cells received an equal amount of PBS. Percentages of IFN-γ^+ cells in total DC (**A**) or total T cells (**B**) from n=3 healthy donors are shown. Cells were gated for HLA-DR$^+$CD11c$^+$ (**A**) or CD3$^+$ (**B**) and IFN-γ staining was performed after cell permeabilization. Data are presented as means ± SEM; *, $p < 0.05$ vs. PBS stimulation. (**C**) Immunomodulatory effects of compound **14** as assessed by the down-regulation of pro- and the up-regulation of anti-inflammatory cytokines. Cytokine quantification in cell culture supernatants from PBMC of healthy human donors after activation with PMA/Iono and stimulation with compounds **12** or **14**. Data from n=3 donors are shown (*$p < 0.05$ vs. PBS). (**D**) Percentages of IFN-γ^+ cells in total bone-marrow-derived DC (bmDC) from n=5 wild-type (WT) or KOR deficient (*Oprk*$^{-/-}$) mice. Cells were gated on MHC-II$^+$CD11c$^+$ and IFN-γ staining was performed after cell permeabilization. Data are presented as means ± SEM; *, $p < 0.05$ vs. PBS. (**E, F**) Flow cytometry of T cells from WT or *Oprk*$^{-/-}$ mice after activation with PMA/Iono and stimulation with compounds **12** or **14**. Representative FACS plots (**E**) and statistics from n=5 mice per group (**F**) are shown. Cells are gated on CD3; data are presented as means ± SEM; *, $p < 0.05$ vs. PBS (**G**) Cytokine secretion in isolated T cells from WT or *Oprk*$^{-/-}$ mice after activation with PMA/Iono and stimulation with compounds **12** or **14**. Data from n=5 mice per group are shown; *$p < 0.05$ vs. PBS.

To assess the anti-inflammatory capacity of the secondary amine **12** and the fluoroethyltriazole derivative **14**, pre-activated T cells and DC were stimulated with both compounds. As shown in Figures 3A and 3B compound **14** significantly reduced the

expression of IFN-γ in human T cells and DC as evidenced by intracellular flow cytometry whereas compound **12** seemed to have only a minor but not significant anti-inflammatory effect on human immune cells (Figures 3A and 3B).

Interestingly, the fluoroethyltriazole **14** might not only have anti-inflammatory properties but also immunomodulatory capacities since besides the down-regulated IFN γ levels in cell culture supernatants from human PBMC stimulated with compound **14**, we detected a significant up-regulation of the anti-inflammatory cytokine IL-10 (Figure 3C). This observation could possibly point to the induction of tolerogenic DC or regulatory T cells by the fluoroethyltriazole **14**. It is well known that opioid receptor agonists are able to modulate immune cell functions. In this context endogenous opioids have been shown to inhibit NF-κB activation in T cells, to induce IL-10 in DC or to prevent DC maturation and thus, reduce their T_H1 priming capacity.[55–57]

DC are central in the regulation of immune responses during autoimmune neuroinflammation since they control the balance between the initiation of immune activation via inducing effector T cells, and immune tolerance via expanding regulatory T cells.[58] In particular IL-10 producing tolerogenic DC, which can be generated by blocking NF-κB signaling, are critically involved in the reprogramming of immune responses during autoimmunity.[59,60] Hence, it might be conceivable that the fluoroethyltriazole **14,** by inducing IL-10 as well as by inhibiting NF-κB activation and the secretion of pro-inflammatory cytokines, could have modulated the immune phenotype. This hypothesis is strengthened by the observation that immunomodulatory properties have already been

described for other kappa opioids. Hu et al. for instance, summarized the immunomodulatory and neuroprotective capacities of KOR ligands in the context of human immunodeficiency virus (HIV) infection.[61]

Next, we assessed whether the anti-inflammatory and immunomodulatory effects of compound **14** were indeed mediated by binding to KOR or whether off-target effects might be detectable. For this purpose, we purified DC and T cells from wild-type mice as well as KOR deficient mouse mutants (*Oprk*$^{-/-}$), activated the cells with PMA/Iono, stimulated them with the secondary amine **12** or the fluoroethyltriazole derivative **14** and quantified cell activation as well as cytokine secretion. As expected, compound **14** significantly down-regualted the IFN-γ secretion in wild-type DC and suppressed the activation of wild-type T cells (Fig. 3D-3F). However, the fluoroethyltriazole derivative **14** had no effect on the cytokine secretion or expression of activation markers in PMA/Iono stimulated DC or T cells from *Oprk*$^{-/-}$ mice (Figures 3D-3F) demonstrating the specificity of compound **14** for KOR. Worth mentioning, similar to human immune cells (Figure 3C) the fluoroethyltriazole **14** showed immunomodulatory properties in wild-type cells since it down-regulated the IFN-γ levels in primary mouse T cells and simultaneously up-regulated the IL-10 expression (Figure 3G). The immunomodulatory capacity of compound **14** was not an off-target effect but dependent on binding to KOR because we did not observe any impact of compound **14** on the cytokine secretion in activated T cells from *Oprk*$^{-/-}$ mice (Figure 3G).

*The fluoroethyltriazole derivative **14** and the secondary amine **12** ameliorated EAE in mice*

To characterize the impact of the fluoroethyltriazole **14** and the secondary amine **12** on the development and perpetuation of inflammatory neurodegeneration *in vivo* and to further assess the therapeutic potential of both compounds, we immunized wild-type mice with myelin oligodendrocyte glycoprotein (MOG) peptide and systemically treated them with compound **12** or **14**. The test compounds **12** and **14** were intraperitoneally injected. In contrast to our *in vitro* observations made in primary mouse immune cells (Figures 3D-3G), the secondary amine **12** delayed disease onset and moreover, reduced EAE severity (Figure 4A). However, the anti-inflammatory effect of the fluoroethyltriazole derivative **14** was even more pronounced since contrary to mice treated with compound **12**, animals that received injections of compound **14** only developed partial tail paralysis (clinical score 1.5-2) and did not show any kind of hind limb paralysis (starting at clinical score 3-4). The beneficial *in vivo* effects of both KOR agonists were mediated by signaling through KOR because treatment of MOG-immunized *Oprk*$^{-/-}$ mice with either of the two compounds did not modulate EAE perpetuation (Figure 4B).

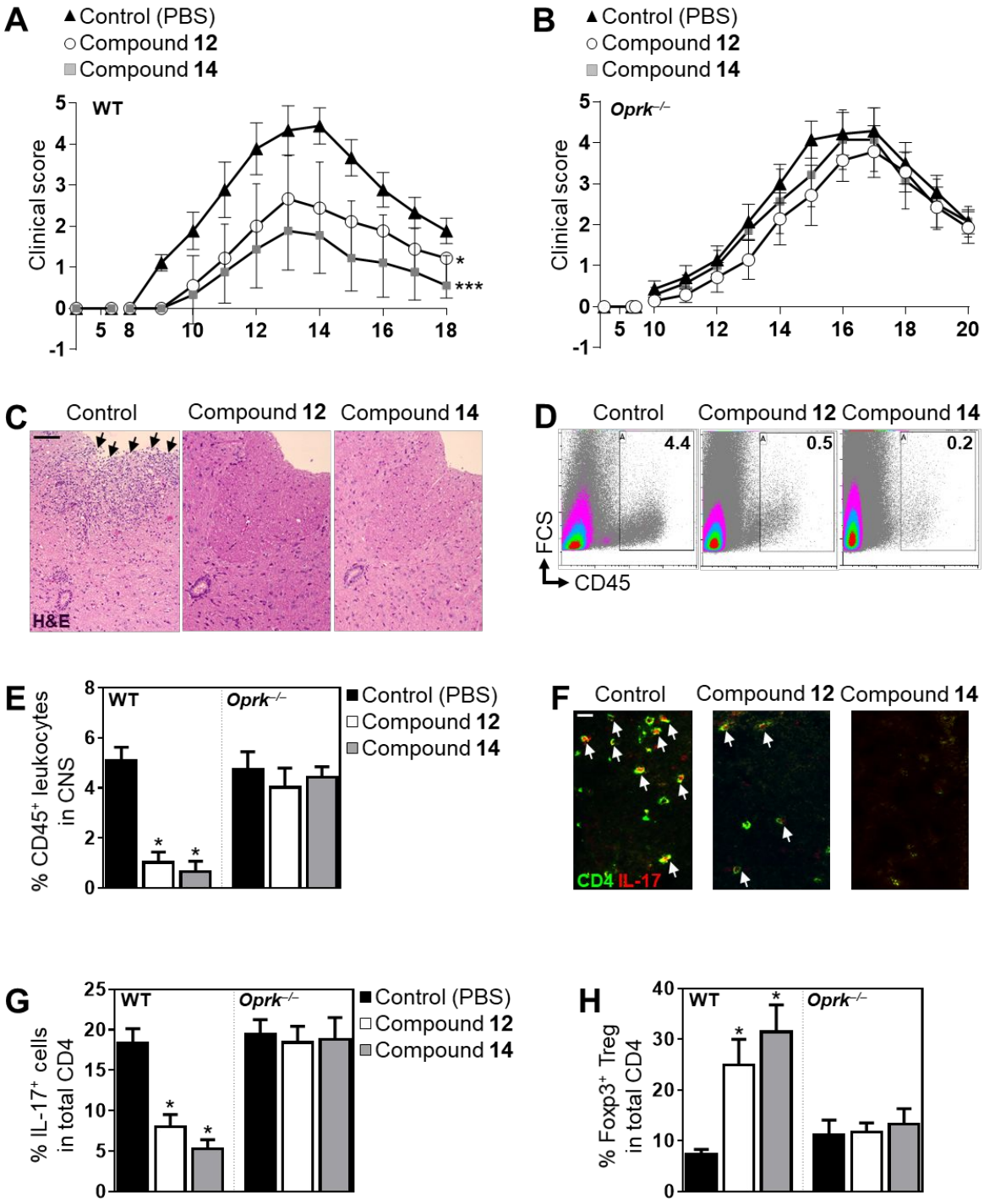

Figure 4: Compounds **12** and **14** reduced severity EAE by down-regulating effector T cell activation. (**A, B**) Wild-type (WT) mice (**A**; n=9 per group) and KOR deficient mutants (*Oprk*$^{-/-}$; **B**; n=7 per group) were immunized with MOG peptide and treated daily with

compounds **12**, **14** (i.p. injection of 100 µl of a 20 µM solution once a day) or PBS starting at day 1 after immunization. Mean clinical scores are shown and data are presented as means ± SEM; *, $p < 0.05$ (day 9-16 after immunization) and ***, $p < 0.01$ vs. PBS-treated controls (day 9-18 after immunization). (**C**) Representative hematoxylin and eosin (H&E) staining in lumbar spinal cord at disease maximum (scale bar, 1 mm). Inflammatory foci and the infiltration of mononuclear cells are indicated by black arrows. (**D, E**) Flow cytometry analyses of total $CD45^+$ leukocytes in the CNS at disease maximum. Representative FACS plots (**D**) and statistics from n=5 mice per group (**E**) are shown. Data are presented as means ± SEM; *, $p < 0.05$ vs. PBS-treated controls; FSC, forward scatter. (**F**, **G**) Immunofluorescence staining (**F**) and flow cytometry (**G**) of $CD4^+IL\text{-}17^+$ effector T cells (T_H17) in the CNS at disease maximum. Representative immunofluorescence staining of lumbar spinal cord tissue using antibodies against CD4 (green) and IL-17 (red) are shown; scale bar, 20 µm; T_H17 cells are indicaed by white arrows (**F**). Statistical evaluation of T_H17 cells in the CNS from n=5 mice per group; data are presented as means ± SEM; *, $p < 0.05$ vs. PBS-treated controls; cells are gated on $CD45^+CD4^+$ and IL-17 staining was performed after cell permeabilization (**G**). (**H**) Flow cytometry of $CD4^+Foxp3^+$ regulatory T cells (Treg) in the CNS at disease maximum. Statistics of Treg numbers from n=5 mice per group are shown, cells are gated on $CD45^+CD4^+$ and Foxp3 staining was performed after cell permeabilization. Data are presented as means ± SEM; *, $p < 0.05$ vs. PBS treatment.

The anti-inflammatory properties of the secondary amine **12** and the fluoroethyltriazole **14** were associated with reduced inflammatory foci and immune cell infiltration into the

CNS of mice treated with both compounds compared to controls that received PBS (Figures 4C-4E). Particularly pathogenic T_H17 cells were hardly detectable in lumbar spinal cord tissue from compound **12**- or compound **14**-treated mice in contrast to PBS-injected controls as evidenced by immunofluorescence staining (Figures 4F and 4G).

Since in our *in vitro* studies we already observed the induction of IL-10 in immune cells stimulated with compound **14** pointing to immunomodulatory properties of this quinoxaline-based KOR agonist and its capacity to induce tolerance besides inhibiting immune activation, we quantified the numbers of immunosuppressive regulatory T cells in the CNS. Interestingly, flow cytometry revealed increased numbers of $CD4^+Foxp3^+$ regulatory T cells in brain and spinal cord tissue from mice treated with compounds **12** and **14** compared to PBS-treated controls (Figure 4H). Again, the anti-inflammatory and immunomodulatory properties were mediated by signaling through KOR and clearly not caused by off-target effects because treatment of mice deficient in KOR did not modulate the immune cell infiltration into the CNS, the numbers of pathogenic T_H17 cells in lumbar spinal cord or the levels of immunosuppressive regulatory T cells (Figures 4D-4H). Thus, these data demonstrate that both quinoxaline-based KOR agonists, the fluoroethyltriazole **14** and the secondary amine **12,** were able to significantly ameliorate neuroinflammation in the mouse model of MOG-induced EAE by down-regulating the expression of pro-inflammatory cytokines in T cells and reducing the infiltration of pathogenic effector cells into the CNS, potentially via expanding or generating immunosuppressive $Foxp3^+$ regulatory T cells.

It has already been suggested that the endogenous opioid system contributes to the pathogenesis of MS and its animal model EAE. Accordingly, Du et al. demonstrated an increased disease severity in MOG-induced EAE in the absence of KOR and convincingly showed alleviated symptoms in response to the activation of KOR with an agonist.[20] Pharmacological activation of KOR with the selective agonists U-50,488 and asimadoline markedly decreased the cumulative clinical score, which was mediated by reduced leukocyte infiltration into the spinal cord.[20] However U-50,488, in contrast to the fluoroethyltriazole derivative **14** or the secondary amine **12**, did neither affect the percentage of pathogenic T_H1 or T_H17 cells in the CNS nor did U-50,488 modulate the cytokine secretion in these cells or show any immunomodulatoy capacity bringing the authors to the conclusion that U-50,488 seemed to play a minor role in the immune system.[20] Instead, in a non-immune-mediated model of demyelination, where mice were fed with a 0.2 % cuprizone diet, the authors identified a remyelinating effect of U-50,488 since this KOR agonist was able to promote the differentiation of myelinated oligodendrocytes from oligodendrocyte precursor cells.[20] The discrepancy in the cellular and molecular mechanisms underlying the beneficial effects of U-50,488 and compounds **12** as well as **14** might be explained by the different chemical structures. U-50,488 penetrates the blood-brain barrier and enters the CNS very fast where it can exert direct neuroprotective effects. The fluoroethyltriazole derivative **14** and the secondary amine **12** are considerably more polar, which results in reduced penetration of the BBB and renders neuroprotective effects unlikely. On the other hand, quinoxalines have been shown to modulate NF-κB signaling in immune cells, such as macrophages, or to inhibit T cell proliferation [62,63] suggesting that the different chemical structures of the KOR agonists

might account for their different effects whereas quinoxaline-based KOR agonists are particularly able to modulate the phenotype and function of immune cells.

3. Conclusion

The immunological processes triggering MS or its animal model EAE involve pathogenic T_H1 and T_H17 cells. These autoreactive T cells are generated in the periphery and infiltrate into the CNS, where they are re-stimulated by antigen-presenting cells, finally leading to local expansion and tissue damage to oligodendrocytes. Interestingly, previous work identified the lung as a niche, where activated, myelin-reactive T cells are stimulated, strongly proliferate and acquire migratory properties to enter the CNS and induce paralysis. Thus, peripheral organs seem to contribute to the activation of autoreactive T cells, their transition into a migratory state as important prerequisites to enter their target tissues. Accordingly, modulation of T cell activation and blockade of their migratory capacities in the periphery might be a promising concept to treat inflammatory CNS diseases. Since it has recently been shown that KOR is expressed on pathogenic T cells and since we were able to confirm the anti-inflammatory potential of decahydroquinoxaline-based KOR agonists in immune cells, we intended to develop novel KOR agonists for the treatment of neuroinflammation. Here, we demonstrated that the newly designed KOR agonists the fluoroethyltriazole derivative **14** and the secondary amine **12** acting predominantly in the periphery, exhibit potent anti-inflammatory and immunomodulatory capacities in primary mouse and human immune cells. Moreover, in MOG-induced EAE compounds **12** and **14**, via signalling through KOR, were able to almost completely protect mice from disease perpetuation. Thus, particularly the fluoroethyltriazole derivative **14** might be a promising candidate for further clinical

development towards a new therapeutic option for the treatment of neuroinflammatory diseases such as MS.

4. Experimental

4.1. Chemistry, General Methods

Oxygen and moisture sensitive reactions were carried out under nitrogen, dried with silica gel with moisture indicator (orange gel, Merck) and in dry glassware (Schlenk flask or Schlenk tube). All solvents were of analytical grade quality. Flash chromatography (FC): Silica gel 60, 40–63 µm (Merck); parentheses include: diameter of the column (ø), length of the stationary phase (l), fraction size (v) and eluent. NMR: NMR spectra were recorded on Agilent DD2 400 MHz and 600 MHz spectrometers; chemical shifts (δ) are reported in parts per million (ppm) against the reference substance tetramethylsilane and calculated using the solvent residual peak of the undeuterated solvent. HPLC method to determine the purity of compounds: Equipment 1: Pump: L-7100, degasser: L-7614, autosampler: L-7200, UV detector: L-7400, interface: D-7000, data transfer: D-line, data acquisition: HSM-Software (all from LaChrom, Merck Hitachi); Equipment 2: Pump: LPG-3400SD, degasser: DG-1210, autosampler: ACC-3000T, UV-detector: VWD-3400RS, interface: DIONEX UltiMate 3000, data acquisition: Chromeleon 7 (Thermo Fisher Scientific); column: LiChropher® 60 RP-select B (5 µm), LiChroCART® 250-4 mm cartridge; flow rate: 1.0 mL/min; injection volume: 5.0 µL; detection at λ = 210 nm; solvents: A: demineralized water with 0.05 % (V/V) trifluoroacetic acid, B: acetonitrile with 0.05 % (V/V) trifluoroacetic acid; gradient elution (% A): 0 - 4 min: 90 %; 4 - 29 min: gradient from 90 % to 0 %; 29 - 31 min: 0 %; 31 - 31.5min: gradient from 0 % to 90 %; 31.5 - 40 min: 90 %. The purity of all test compounds is greater than 95 %.

4.2. Synthetic procedures

2-(3,4-Dichlorophenyl)-1-[(4a*SR*,8*SR*,8a*SR*)-8-(pyrrolidin-1-yl)-3,4,4a,5,6,7,8,8a-octahydroquinoxaline-1(2*H*)-yl]ethan-1-one (12)

TFA (0.4 mL, 5.1 mmol, 32 eq) was added dropwise to a solution of **11** (81 mg, 0.16 mmol, 1 eq) in CH_2Cl_2 (3 mL). The mixture was stirred at rt for 18 h. After addition of toluene, the solvents were removed in vacuo (azeotropic distillation). Then, NaOH (0.5 M, 10 mL) was added and the mixture was extracted with CH_2Cl_2 (2 x 20 mL). After removal of the solvent in vacuo, the residue was purified by flash column chromatography (Ø = 3 cm, h =8 cm, $CH_2Cl_2/CH_3OH/NH_3$ (25 %) 94:5:1, V = 12 mL, R_f = 0.48 ($CH_2Cl_2/CH_3OH/NH_3$ (25 %) 89:10:1). Yellow oil, yield 64 mg (98 %). $C_{20}H_{27}Cl_2N_3O$ (396,4 g/mol). ^{1}H NMR (400 MHz, $CDCl_3$): δ [ppm] = 1.23 – 1.37 (m, 1H, 5-C*H*$_2$), 1.51 – 1.73 (m, 8H, 6-C*H*$_2$, 7-C*H*$_2$, N(CH_2C*H*$_2$)$_2$), 1.81 – 2.07 (m, 1H, 5-C*H*$_2$), 2.46 – 2.88 (m, 5H, 3-C*H*$_2$, N(C*H*$_2$$CH_2$)$_2$), 2.96 – 3.07 (m, 2H, 3-C*H*$_2$, 8-C*H*), 3.09 – 3.21 (m, 1H, 2-C*H*$_2$), 3.27 – 3.54 (m, 2H, 2-C*H*$_2$, 4a-C*H*), 3.62 – 3.83 (m, 2H, C(=O)C*H*$_2$-aryl), 4.36 – 4.65 (m, 1H, 8a-C*H*), 7.15 – 7.23 (m, 1H, 6-C*H*$_{arom}$), 7.29 – 7.42 (m, 2H, 2-C*H*$_{arom}$, 5-C*H*$_{arom}$). A signal for the 4-N*H* proton is not seen in the spectrum.

2-(3,4-dichlorophenyl)-1-[(4a*RS*,8*RS*,8a*SR*)-4-(prop-2-yn-1-yl)-8-(pyrrolidin-1-yl)-3,4,4a,5,6,7,8,8a-octahydroquinoxalin-1(2*H*)-yl]ethan-1-one (13h)

Under N_2 atmosphere, propargyl bromide (80% wt solution in toluene, 29 µL, 0.3 mmol, 1.2 eq) was added to a suspension of **12** (100 mg, 0.25 mmol, 1 eq) and Cs_2CO_3 (163 mg, 0.5 mmol, 2 eq) in dry DMF (1.5 mL). The mixture was stirred at 40 °C for 6 h. After filtration over silica gel, the solvent was removed in vacuo. Afterwards the residue

was dissolved in CH_2Cl_2 (20 mL) and the solution was washed with brine (3 x 20 mL). The organic layer was dried (Na_2SO_4), filtered and concentrated in vacuo. The residue was purified by flash column chromatography (Ø = 2 cm, h = 15 cm, $CH_2Cl_2/CH_3OH/NH_3$ (25 %) 96:3:1, V = 12 mL, R_f = 0.66 ($CH_2Cl_2/CH_3OH/NH_3$ (25 %) 94:5:1)). Pale yellow oil, yield 100 mg (92 %). $C_{23}H_{29}Cl_2N_3O$ (434.4 g/mol). ^{1}H NMR (600 MHz, $CDCl_3$): δ (ppm) = 1.29 – 1.50 (m, 3H, 5-C*H*$_2$, 6-C*H*$_2$,7-C*H*$_2$), 1.52 – 1.75 (m, 5H, 6-C*H*$_2$, N(CH_2C*H*$_2$)$_2$), 1.83 – 2.08 (m, 2H, 5-C*H*$_2$,7-C*H*$_2$), 2.19 (s, 1H, NCH_2C≡C*H*), 2.43 – 2.80 (m, 7H, N(C*H*$_2$CH_2)$_2$, 3-C*H*$_2$, 8-C*H*), 3.19 – 3.60 (m, 5H, 2-C*H*$_2$, C*H*$_2$C≡CH, 4a-C*H*), 3.62 – 3.84 (m, 2H, C(=O)C*H*$_2$-aryl), 4.37 – 4.64 (m, 1H, 8a-C*H*), 7.06 – 7.24 (m, 1H, 6-C*H*$_{arom}$), 7.32 – 7.41 (m, 2H, 2-C*H*$_{arom}$, 5-C*H*$_{arom}$).

2-(3,4-Dichlorophenyl)-1-[(4a*RS*,8*RS*,8a*SR*)-4-{[1-(2-fluoroethyl)-1*H*-1,2,3-triazol-4-yl]methyl}-8-(pyrrolidin-1-yl)-3,4,4a,5,6,7,8,8a-octahydroquinoxalin-1(2*H*)-yl]ethan-1-one (14)

Under N_2 atmosphere, NaN_3 (97 mg, 1.5 mmol, 7.5 eq) was added to a solution of (2-fluoroethyl) tosylate (234 mg, 1 mmol, 5 eq) in dry DMF (7 mL). The mixture was stirred at rt for 48 h. Afterwards, the solution was heated at 40 °C and the formed 1-azido-2-fluoroethane was directly distilled into a solution of **13h** (85 mg, 0.2 mmol, 1 eq), $CuSO_4 \cdot 5H_2O$ (45 mg, 0.18 mmol, 0.9 eq) and sodium ascorbate (67 mg, 0.34 mmol, 1.7 eq) in DMF (3 mL) and H_2O (2 mL). A constant flow of N_2 was used to facilitate the transfer of 1-azido-2-fluoroethane. After 2 h, brine (20 mL) was added and the mixture was extracted with CH_2Cl_2 (3 x 15 mL). The combined organic layers were dried (Na_2SO_4), filtered and concentrated in vacuo. The residue was purified by flash column chromatography (Ø = 2 cm, h = 15 cm, $CH_2Cl_2/CH_3OH/NH_3$ (25 %) 89:9:1, V = 12 mL, R_f

= 0.40 (CH_2Cl_2/CH_3OH/NH_3 (25 %) 94:5:1)). Colorless oil, yield 31 mg (30 %). $C_{25}H_{33}Cl_2FN_6O$ (523.5 g/mol). ^{1}H NMR (600 MHz, $CDCl_3$): δ (ppm) = 1.30 – 1.46 (m, 2H, 7-CH_2, 5-CH_2), 1.55 – 1.75 (m, 6H, 6-CH_2, N(CH_2CH_2)$_2$), 1.87 – 2.12 (m, 1H, 7-CH_2), 2.21 (td, *J* = 11.9/3.7 Hz, 1H, 3-CH_2), 2.26 – 2.35 (m, 1H, 5-CH_2), 2.39 – 2.86 (m, 6H, N(CH_2CH_2)$_2$, 8-C*H*, 3-CH_2), 3.18 – 3.38 (m, 2H, 2-CH_2), 3.46 – 3.68 (m, 3H, C(=O)CH_2-aryl, 4a-C*H*), 3.72 – 3.97 (m, 2H, NCH_2-triazole), 4.28 – 4.59 (m, 1H, 8a-C*H*), 4.67 (dt, *J* = 27.4/4.3 Hz, 2H, CH_2CH_2F), 4.80 (dt, *J* = 46.8/5.0 Hz, 2H, CH_2CH_2F), 7.00 – 7.21 (m, 1H, 6-CH_{arom}), 7.28 – 7.36 (m, 2H, 2-CH_{arom}, 5-CH_{arom}), 7.48 (d, *J* = 1.0 Hz, 1H, 5-C$H_{triazole}$).

2-(3,4-Dichlorophenyl)-1-((4a*RS*,8*RS*,8a*SR*)-4-{2-[4-(3-fluoropropyl)-1*H*-1,2,3-triazol-1-yl]acetyl}-8-(pyrrolidin-1-yl)-3,4,4a,5,6,7,8,8a-octahydroquinoxalin-1(2*H*)-yl)ethan-1-one (18)

Pent-4-yn-1-yl 4-methylbenzenesulfonate (250 mg, 1.1 mmol, 5 eq) was added to a solution of TBAF·3H_2O (827 mg, 2.6 mmol, 12.5 eq) in H_2O (0.3 mL). The mixture was stirred at 45 °C for 2 h. Afterwards, the solution was heated at 100 °C and the formed 5-fluoropent-1-yne was directly distilled into a solution of **17** (160 mg, 0.3 mmol, 1 eq), $CuSO_4$·5H_2O (75 mg, 0.3 mmol, 0.9 eq) and sodium ascorbate (113 mg, 0.6 mmol, 1.7 eq) in DMF (2.5 mL) and H_2O (1 mL). A constant flow of N_2 was used to facilitate the transfer of 5-fluoropent-1-yne. After 3 h, H_2O (15 mL) was added and the mixture was extracted with CH_2Cl_2 (3 x 10 mL). The combined organic layers were dried (Na_2SO_4), filtered and concentrated in vacuo. The residue was purified by flash column chromatography (Ø = 2 cm, h = 15 cm, CH_2Cl_2/CH_3OH/NH_3 (25 %) 97:2:1 → 89:10:1, V = 12 mL, R_f = 0.52 (CH_2Cl_2/CH_3OH/NH_3 (25 %) 89:10:1)). Pale yellow oil, yield 31 mg

(17 %). $C_{27}H_{35}Cl_2FN_6O_2$ (565.5 g/mol). ^{1}H NMR (600 MHz, $CDCl_3$): δ (ppm) = 1.44 – 1.97 (m, 12H, 5-CH_2, 6-CH_2, 7-CH_2, N(CH_2CH_2)$_2$, N(CH_2CH_2)$_2$), 2.00 – 2.19 (m, 2H, $CH_2CH_2CH_2F$), 2.51 – 2.74 (m, 3H, 8-CH, N(CH_2CH_2)$_2$), 2.87 (t, J = 7.5 Hz, 2H, $CH_2CH_2CH_2F$), 3.50 – 3.81 (m, 5H, 2-CH_2, 3-CH_2, C(=O)CH_2-aryl), 3.86 – 4.01 (m, 2H, 3-CH_2, 4a-CH), 4.50 (dt, J = 47.2/5.9 Hz,, 1H, $CH_2CH_2CH_2F$), 4.47 – 4.53 (m, 1H, 8a-CH), 5.10 – 5.26 (m, 2H, C(=O)CH_2-triazole), 7.08 (dd, J = 8.3/2.1 Hz, 1H, 6-CH_{arom}), 7.33 (d, J = 2.1 Hz, 1H, 2-CH_{arom}), 7.40 (d, J = 8.2 Hz, 1H, 5-CH_{arom}), 7.51 (s, 1H, 5-C$H_{triazole}$).

4.3. Receptor binding studies

Materials, preparation of membrane homogenates from various tissues, protein determination, and the generatl procedure for binding assays are detailed in the Supportin Information.

Determination of KOR affinity (guinea pig brain)

The assay was performed with the radioligand [^{3}H]U-69,593 (55 Ci/mmol, Amersham, Little Chalfont, UK). The thawed guinea pig brain membrane preparation (about 100 µg of the protein) was incubated with various concentrations of test compounds, 1 nM [^{3}H]U-69,593, and TRIS-$MgCl_2$-Puffer (50 mM, 8 mM $MgCl_2$, pH 7.4) at 37 °C. The non-specific binding was determined with 10 µM unlabeled U-69,593. The K_d-value of U-69,593 is 0.69 nM.

4.4. *In vitro* functional assays

cAMP inhibition assay

To measure KOR $G_{\alpha i}$-mediated cAMP inhibition, HEK 293T (ATCC CRL-11268) cells were co-transfected with human KOR along with a luciferase-based cAMP biosensor (GloSensor; Promega) and assays were performed similar to previously described.[66] After 16 h, transfected cells were plated into Poly-lysine coated 384-well white clear bottom cell culture plates with DMEM + 1% dialyzed FBS at a density of 15,000-20,000 cells per 40 µl per well and incubated at 37 °C with 5% CO_2 overnight. The next day, drug solutions were prepared in fresh drug buffer [20 mM HEPES, 1X HBSS, 0.3% bovine serum album (BSA), pH 7.4] at 3X drug concentration. Plates were decanted and received 20 µl per well of drug buffer (20 mM HEPES, 1X HBSS) followed by addition of 10 µl of drug solution (3 wells per condition) for 15 min in the dark at room temperature. To stimulate endogenous cAMP via β adrenergic-Gs activation, 10 µl luciferin (4 mM final concentration) supplemented with isoproterenol (400 nM final concentration) were added per well. Cells were again incubated in the dark at room temperature for 15 min, and luminescence intensity was quantified using a Wallac TriLux microbeta (Perkin Elmer) luminescence counter. Results (relative luminescence units) were plotted as a function of drug concentration, normalized to % SalA stimulation, and analyzed using “log(agonist) vs. response” in GraphPad Prism 5.0.

Tango β-arrestin-2 recruitment assay

The KOR Tango constructs were designed and assays were performed as previously described.[67,68] HTLA cells expressing TEV fused-β-arrestin2 (kindly provided by Dr. Richard Axel, Columbia Univ.) were transfected with the KOR Tango construct. The next

day, cells were plated in DMEM supplemented with 1% dialyzed FBS in poly-L-lysine coated 384-well white clear bottom cell culture plates at a density of 10,000-15,000 cells/well in a total of 40 µl. The cells were incubated for at least 6 h before receiving drug stimulation. Drug solutions were prepared in drug buffer (20 mM HEPES, 1X HBSS, 0.3% BSA, pH 7.4) at 3X and added to cells (20 µl per well) for overnight incubation. Drug solutions used for the Tango assay were exactly the same as used for the cAMP assay. The next day, media and drug solutions were removed and 20 µl per well of BrightGlo reagent (purchased from Promega, after 1:20 dilution) was added. The plate was incubated for 20 min at room temperature in the dark before being counted using a luminescence counter. Results (relative luminescence units) were plotted as a function of drug concentration, normalized to % SalA stimulation, and analyzed using "log(agonist) vs. response" in GraphPad Prism 5.0.

4.5. *In vitro* studies to assess the anti-inflammatory activity in immune cells

Immune cell isolation and stimulation

C57BL/6 mice (wild-type; purchased from Janvier Labs, Le Genest-Saint-Isle, France) and kappa-opioid receptor deficient mouse mutants (*Oprk*$^{-/-}$, purchased from The Jackson Laboratory, Bar Harbor, ME) were used at the age of 8 to 12 weeks and housed under specific pathogen–free conditions in microisolator cages. Mice were given chow and water *ad libitum* and animal experiments were performed with the approval of the State Review Board of North Rhine-Westphalia according to the German law for animal welfare (reference numbers 81-02.05.50.17.015 and 84-02.05.20.11.227). After sacrifice of mice peripheral lymph nodes, femurs and tibias were removed to isolate T cells or bone marrow cells (see below). Single cell suspensions of mouse lymph nodes were prepared

according to standard methods. Subsequently, total T cells were isolated from cell suspensions using the Pan T Cell Isolation Kit II (Miltenyi Biotech, Bergisch Gladbach, Germany) and subjected to flow cytometry analyses or were activated for 12 h with phorbol 12-myristate 13-acetate (PMA, 5 ng/ml) and ionomycin (500 ng/ml) and cultured for 48 h in the presence of compound **12**, compound **14** (1 µg/ml each) or PBS as a control.

Human DC and T cells were isolated from peripheral blood mononuclear cells (PBMC). Therefore, PBMC were purified from 20 ml of heparinized blood, obtained with the informed consent from healthy donors by Ficoll gradient centrifugation according to standard methods (Ficoll reagent was purchased from Merck, Darmstadt, Germany). Total DC or T cells were negatively enriched using the Pan-DC Enrichment Kit or the Pan T Cell Isolation Kit (Miltenyi Biotech). All experiments were carried out according to the declaration of Helsinki and were approved by the ethical committee of the University of Münster Medical School (2008-180-f-S). After isolation human DC and T cells were activated for 12 h with PMA (5 ng/ml) and ionomycin (500 ng/ml) and cultured for additional 48 h in the presence of compound **12**, compound **14** (1 µg/ml each) or PBS (as a control) and finally subjected to flow cytometry analyses or cytokine quantifiaction (see below).

Generation of mouse bone marrow-derived dendritic cells (bmDC)

BmDC were generated as described.[69] Bone marrow was collected from tibias and femurs of wild-type and *Oprk*$^{-/-}$ mice, single cell suspensions were prepared and cultured in the presence of 150 U/ml GM-CSF and 75 U/ml IL-4 (Biotechne, Minneapolis, MN) for 9 days.

From day 7 to day 9 of culture, cells were stimulated with PMA (5 ng/ml) and ionomycin (500 ng/ml) in the presence or absence of compound **12** or compound **14** (1 µg/ml each). On day 9, bmDC were harvested and used for flow cytometry analyses.

4.6. *In vivo* experiments to characterize the efficacy of compounds 12 and 14

Induction of EAE

C57BL/6 mice (wild-type; purchased from Janvier Labs) and *Oprk*$^{-/-}$ mutant mice (purchased from The Jackson Laboratory) were used at the age of 8 to 12 weeks, housed under specific pathogen–free conditions, given chow and water *ad libitum*, and monitored for clinical signs daily. Animal experiments were approved by the State Review Board of North Rhine-Westphalia (reference no. 84-02.04.2013-A139). EAE was induced by subcutaneous injection of 200 mg of MOG peptide (MEVGWYRSPFSRVVHLYRNGK; Charité, Berlin, Germany) emulsified in complete Freund's adjuvant (Merck, Darmstadt, Germany) containing 200 mg of Mycobacterium tuberculosis H37RA (Fisher Scientific, Hampton, NH). Pertussis toxin (400 ng; Enzo Life Sciences, Lörrach, Germany) in 200 ml of PBS was injected intraperitoneally at the day of immunization and 2 days later. Disease severity was scored daily in a blinded fashion by two independent investigators using a scale from 0 to 10 (experimental autoimmune neuritis score).[51,70] Compounds **12** and **14** were injected intraperitoneally starting 1 day after immunization (100 µl of a 20 µM solution). Control mice received an equal amount of PBS (Fisher Scientific). At the peak of disease (days 12-15 after immunization in wild-type and days 14-18 after immunization in *Oprk*$^{-/-}$ mice) part of the mice were sacrificed and analyzed by histology (see below) or flow cytometry (see above). For flow cytometry mononuclear cells from the CNS (brain and spinal cord) were isolated. Therefore, mice were perfused with PBS through the left

ventricle and subsequently, tissues were homogenized through 100 µm cell strainers to obtain single-cell suspensions, and Percoll gradient centrifugation was performed to enrich leukocytes. For histology mouse brain and spinal cord tissues were cryopreserved in NEG-50 (Fisher Scientific) or fixed with formalin.

Histology and immunofluorescence staining

For Hematoxylin and Eosin (H&E) staining, tissues were embedded in paraffin after formalin fixation and cut into 3 µm sections. Following deparaffinization using standard protocols, H&E staining was performed using an autostainer (Tissue-Tek Prisma, Sakura Finetek, Alphen aan den Rijn, The Netherlands). Subsequently, slides were analyzed on an Olympus BX63 microscope using cellSens software (Olympus, Münster, Germany). For immunofluorescence staining cryopreserved mouse brain and spinal cord tissues were cut into 3 µm sections, and immunofluorescence staining was performed using standard methods and the appropriate dilutions of primary antibodies against CD4 (clone RM4-5, purchased from Biolegend) and IL-17A (clone eBio17B7, purchased from Thermo Fisher Scientific). Subsequently, slides were incubated with Alexa Fluor (AF) 594- or 488-coupled secondary antibodies (Life Technologies, Carlsbad, CA). Isotype controls were included in each staining.

Statistics

All values are expressed as means ± SEM. Statistically significant differences were assessed by one-way analysis of variance (ANOVA) test, comparing more than two groups. The alpha-level was set at a value of <0.05 in most and at a value of <0.01 in

exceptional cases (e.g. Fig. 4A). SigmaPlot 12 or GraphPad Prism 7 was used to analyze, plot, and illustrate data.

Animal experiments

All animal experiments were performed with the approval of the State Review Board of North Rhine-Westphalia according to the German law for animal welfare. Reference numbers 81-02.05.50.17.015 and 84-02.05.20.11.227 and 84-02.04.2013-A139.

Supporting Information

Supporting Information contains purity data of all compounds. Moreover, parts of the experimental part including synthetic procedures, molecular modelling and pharmacological studies are given. The ^{1}H and ^{13}C NMR spectra of all synthesized compounds are included. Molecular Formula Strings are added. This material is available free of charge via the Internet at http://pubs.acs.org.

Author Information

Corresponding author

*Tel: +49-251-8333311. Fax: +49-8332144. Email: wuensch@uni-muenster.de

Acknowledgement

Financial support of this project by the *Deutsche Forschungsgemeinschaft (DFG*, SFB-TR 128 project A10 to K.L., SFB 1009 project B07 to K.L., project 817/5-1 to K.L., Cluster of excellence Cells in Motion, project FF-2016-11 to K.L. and B.W.) as well as the Interdisciplinary Center for Clinical Research (IZKF, project Lo2/004/16 to K.L.) is

gratefully acknowledged. Support was also given by NIDA (Grant PO1 DA035764 to T.C. and the NIMH Psychoactive Drug Screening Program for binding assays. We would like to thank Meike Steinert and Kerstin Vischedyk for excellent technical assistance.

Conflict of interest

The authors declare no conflict of interests.

Abbreviations Used

APCI	atmospheric pressure chemical ionization
BBB	blood brain barrier
bmDC	bone marrow-derived dendritic cells
CNS	central nervous system
CSF	cerebrospinal fluid
DC	dendritic cells
DOR	δ opioid receptor
EAE	experiental autoimmune encephalomyelitis
GLAT	glatiramer acetate
H&E	hematoxylin and eosin
HIV	human immunodeficiency virus
INF-β	interferone β
INF-γ	interferone γ
INL-17	interleukin-17
Iono	ionomycin
KOR	κ opioid receptor

l	length of the stationary phase
MOG	myelin oligodendrocyte glycoprotein
MOR	μ opioid receptor
MS	multiple sclerosis
OPC	oligodendrocyte progenitor cells
PBMC	peripheral blood mononuclear cells
PMA	phorbol 12-myristate 13-acetate
PML	progressive multifocal leukoencephalopathy
S1P	sphingosine-1-phosphate
TBAF	tetrabutylammonium fluoride
TBDPS	*tert*-butyldiphenylsilyl
T_H1	T helper cells 1
T_H17	T helper cells 17
Treg	regulatory T cells
V	fraction size
WT	wild-type

References

(1) Browne, P.; Chandraratna, D.; Angood, C.; Tremlett, H.; Baker, C.; Taylor, B. V.; Thompson, A. J. Atlas of multiple sclerosis 2013: a growing global problem with widespread inequity. *Neurology* **2014**, *83* (11), 1022–1024.

(2) Baecher-Allan, C.; Kaskow, B. J.; Weiner, H. L. Multiple sclerosis: mechanisms and immunotherapy. *Neuron* **2018**, *97* (4), 742–768.

(3) Hemmer, B.; Kerschensteiner, M.; Korn, T. Role of the innate and adaptive immune responses in the course of multiple sclerosis. *Lancet Neurol.* **2015**, *14* (4), 406–419.

(4) Odoardi, F.; Sie, C.; Streyl, K.; Ulaganathan, V. K.; Schläger, C.; Lodygin, D.; Heckelsmiller, K.; Nietfeld, W.; Ellwart, J.; Klinkert, W. E. F.; Lottaz, C.; Nosov, M.; Brinkmann, V.; Spang, R.; Lehrach, H.; Vingron, M.; Welkerle, H.; Flugel-Koch, C.; Flugel, A. T Cells become licensed in the lung to enter the central nervous system. *Nature* **2012**, *488* (7413), 675–679.

(5) Koutrolos, M.; Berer, K.; Kawakami, N.; Wekerle, H.; Krishnamoorthy, G. Treg cells mediate recovery from EAE by controlling effector T cell proliferation and motility in the CNS. *Acta Neuropathol. Commun.* **2014**, *2*, 163.

(6) Venken, K.; Hellings, N.; Broekmans, T.; Hensen, K.; Rummens, J.-L.; Stinissen, P. Natural naive CD4+CD25+CD127low regulatory T cell (Treg) development and function are disturbed in multiple sclerosis patients: recovery of memory Treg homeostasis during disease progression. *J. Immunol.* **2008**, *180* (9), 6411–6420.

(7) Frisullo, G.; Nociti, V.; Iorio, R.; Patanella, A. K.; Caggiula, M.; Marti, A.; Sancricca, C.; Angelucci, F.; Mirabella, M.; Tonali, P. A.; Batocchi, A.P. Regulatory T cells fail to suppress CD4 + T-Bet + T cells in relapsing multiple

sclerosis patients. Immunology 2009, 127 (3), 418–428.

(8) Chen, X.; Winkler-Pickett, R. T.; Carbonetti, N. H.; Ortaldo, J. R.; Oppenheim, J. J.; Howard, O. M. Z. Pertussis toxin as an adjuvant suppresses the number and function of CD4+CD25+ T regulatory cells. *Eur. J. Immunol.* **2006**, *36* (3), 671–680.

(9) Haghikia, A.; Hohlfeld, R.; Gold, R.; Fugger, L. Therapies for multiple sclerosis: translational achievements and outstanding needs. *Trends Mol. Med.* **2013**, *19* (5), 309–319.

(10) Weiner, H. L. The Challenge of multiple sclerosis: how do we cure a chronic heterogeneous disease? *Ann. Neurol.* **2009**, *65* (3), 239–248.

(11) Comabella, M.; Río, J.; Espejo, C.; Ruiz de Villa, M.; Al-zayat, H.; Nos, C.; Deisenhammer, F.; Baranzini, S. E.; Nonell, L.; López, C.; Julià, E.; Oksenberg, J.E.; Montalban, X. Changes in matrix metalloproteinases and their inhibitors during interferon-beta treatment in multiple sclerosis. *Clin. Immunol.* **2009**, *130* (2), 145–150.

(12) Lalive, P. H.; Neuhaus, O.; Benkhoucha, M.; Burger, D.; Hohlfeld, R.; Zamvil, S. S.; Weber, M. S. Glatiramer acetate in the treatment of multiple sclerosis. *CNS Drugs* **2011**, *25* (5), 401–414.

(13) Conway, D.; Cohen, J. A. combination therapy in multiple sclerosis. *Lancet Neurol.* **2010**, *9* (3), 299–308.

(14) Miron, V. E.; Ludwin, S. K.; Darlington, P. J.; Jarjour, A. A.; Soliven, B.; Kennedy, T. E.; Antel, J. P. Fingolimod (FTY720) enhances remyelination following demyelination of organotypic cerebellar slices. *Am. J. Pathol.* **2010**, *176* (6), 2682–2694.

(15) Ghoreschi, K.; Brück, J.; Kellerer, C.; Deng, C.; Peng, H.; Rothfuss, O.; Hussain, R. Z.; Gocke, A. R.; Respa, A.; Glocova, I.; Valtcheva, N.; Alexander, E.; Feil, S.; Feil, R.; Schulze-Osthoff, K.; Rupec, R.A.; Lovett-Racke, A.E.; Dringen, R.; Racke, M.K.; Röcken, M. Fumarates improve psoriasis and multiple sclerosis by inducing type II dendritic cells. *J. Exp. Med.* **2011**, *208* (11), 2291–2303.

(16) Wenning, W.; Haghikia, A.; Laubenberger, J.; Clifford, D. B.; Behrens, P. F.; Chan, A.; Gold, R. Treatment of progressive multifocal leukoencephalopathy associated with matalizumab. *N. Engl. J. Med.* **2009**, *361* (11), 1075–1080.

(17) Lindå, H.; von Heijne, A.; Major, E. O.; Ryschkewitsch, C.; Berg, J.; Olsson, T.; Martin, C. Progressive multifocal leukoencephalopathy after natalizumab monotherapy. *N. Engl. J. Med.* **2009**, *361* (11), 1081–1087.

(18) Tillery, E. E.; Clements, J. N.; Howard, Z. Updates in drug therapy review of drugs/pharmacotheray. Open Access What's New in Multiple Sclerosis? *Ment Heal. Clin* **2017**, *7* (5), 213–233.

(19) Li, H.; Shi, F.-H.; Huang, S.-Y.; Zhang, S.-G.; Gu, Z.-C.; Wei, J.-F. Clinical adverse effects of natalizumab. m*edicine (Baltimore).* **2018**, *97* (28), e11507.

(20) Du, C.; Duan, Y.; Wei, W.; Cai, Y.; Chai, H.; Lv, J.; Du, X.; Zhu, J.; Xie, X. Kappa opioid receptor activation alleviates experimental autoimmune encephalomyelitis and promotes oligodendrocyte-mediated remyelination. *Nat. Commun.* **2016**, *7*, 11120.

(21) Lynch, J. L.; Alley, J. F.; Wellman, L.; Beitz, A. J. Decreased spinal cord opioid receptor mRNA expression and antinociception in a Theiler's murine encephalomyelitis virus model of multiple sclerosis. *Brain Res.* **2008**, *1191*, 180–191.

(22) Jankovic, B. D. Enkephalins and immune inflammatory reactions. *Acta Neurol. (Napoli).* **1991**, *13* (5), 433–441.

(23) Waldhoer, M.; Bartlett, S. E.; Whistler, J. L. Opioid receptors. *Annu. Rev. Biochem.* **2004**, *73* (1), 953–990.

(24) Bunzow, J. R.; Saez, C.; Mortrud, M.; Bouvier, C.; Williams, J. T.; Low, M.; Grandy, D. K. Molecular cloning and tissue distribution of a putative member of the rat opioid receptor gene family that is not a mu, delta or kappa opioid receptor type. *FEBS Lett.* **1994**, *347* (2–3), 284–288.

(25) Laurence Lalanne; Gulebru Ayranci; Brigitte, L. K.; Lutz, P. E. The kappa opioid receptor: from addiction to depression, and back. *Front. Psychiatry* **2014**, *5* (DEC), 1–17.

(26) Vanderah, T. W. Delta and kappa opioid receptors as suitable drug targets for pain. *Clin. J. Pain* **2010**, *26* (SUPPL.10), 10–15.

(27) Chavkin, C. The Therapeutic potential of κ-opioids for treatment of pain and addiction. *Neuropsychopharmacology* **2011**, *36* (1), 369–370.

(28) Inui, S. Nalfurafine hydrochloride to treat pruritus: a Rrview. *Clin. Cosmet. Investig. Dermatol.* **2015**, *8*, 249.

(29) Li, W.; Sun, H.; Chen, H.; Yang, X.; Xiao, L.; Liu, R.; Shao, L.; Qiu, Z. Major depressive disorder and kappa opioid receptor antagonists. *Transl. Perioper. Pain* Med. **2016**, *1*, 4-16.

(30) Bidlack, J. M. Detection and function of opioid receptors on cells from the immune system. *Clin. Diagn. Lab. Immunol.* **2000**, *7* (5), 719–723.

(31) Bourgeois, C.; Werfel, E.; Galla, F.; Lehmkuhl, K.; Torres-Gómez, H.; Schepmann, D.; Kögel, B.; Christoph, T.; Straßburger, W.; Englberger, W.;

Soeberdt, M.; Hüwel, S.; Galla, H.J.; Wünsch, B. Synthesis and pharmacological evaluation of 5-pyrrolidinylquinoxalines as a novel class of peripherally restricted κ-opioid receptor agonists. *J. Med. Chem.* **2014**, *57* (15), 6845–6860.

(32) Molenveld, P.; Bouzanne Des Mazery, R.; Sterk, G. J.; Storcken, R. P. M.; Autar, R.; Van Oss, B.; Van Der Haas, R. N. S.; Fröhlich, R.; Schepmann, D.; Wünsch, B.; Soeberdt, M. Conformationally restricted κ-opioid receptor agonists: synthesis and pharmacological evaluation of diastereoisomeric and enantiomeric decahydroquinoxalines. *Bioorganic Med. Chem. Lett.* **2015**, *25* (22), 5326–5330.

(33) Soeberdt, M.; Molenveld, P.; Storcken, R. P. M.; Bouzanne Des Mazery, R.; Sterk, G. J.; Autar, R.; Bolster, M. G.; Wagner, C.; Aerts, S. N. H.; Van Holst, F. R.; Wegert, A.; Tangherlini, G.; Frehland, B.; Schepmann, D.; Metze, D.; Lotts, T.; Knie, U.; Lin, K.Y.; Huang, T.Y.; Lai, C.C.; Ständer, S.; Wünsch, B.; Abels, C. Design and synthesis of enantiomerically pure decahydroquinoxalines as potent and selective κ-opioid receptor agonists with anti-inflammatory activity in vivo. *J. Med. Chem.* **2017**, *60*, 2526–2551.

(34) Fontenas, C.; Bejan, E.; Haddou, H. A.; Balavoine, G. G. A. The Boekelheide reaction: trifluoroacetic anhydride as a convenient acylating agent. *Synth. Commun.* **1995**, *25* (5), 629–633.

(35) Krumlinde, P.; Bogár, K.; Bäckvall, J. E. Asymmetrie Synthesis of bicyclic siol serivatives through metal and enzyme catalysis: application to the formal synthesis of sertraline. *Chem. - A Eur. J.* **2010**, *16* (13), 4031–4036.

(36) Nishimura, N.; Norman, M. H.; Liu, L.; Yang, K. C.; Ashton, K. S.; Bartberger, M. D.; Chmait, S.; Chen, J.; Cupples, R.; Fotsch, C.; Helmering, J.; Jordan, S.R.; Kunz, R.K.; Pennington, L.D.; Poon, S.F.; Siegmund, A.; Sivits, G.; Lloyd, D.J.;

Hale, C.; St Jean, D.J. Jr. Small molecule disruptors of the glucokinase-glucokinase regulatory protein interaction: 3. structure-activity relationships within the aryl carbinol region of the N-arylsulfonamido-N'-arylpiperazine series. *J. Med. Chem.* **2014**, *57* (7), 3094–3116.

(37) Wang, Ying. Brewer, Jason T. Akritopoulouzanze, Irini. Djuric, Steven W. Pohlki, Frauke. Braje, Wilfried. Relo, A.-L. Modulators of 5-HT Receptors and Methods of Use thereof. US 2011/0118231 A1, 2010.

(38) Michel, K.; Büther, K.; Law, M. P.; Wagner, S.; Schober, O.; Hermann, S.; Schäfers, M.; Riemann, B.; Höltke, C.; Kopka, K. Development and evaluation of endothelin-A receptor (radio)ligands for positron emission tomography. *J. Med. Chem.* **2011**, *54* (4), 939–948.

(39) Hugenberg, V.; Riemann, B.; Hermann, S.; Schober, O.; Schäfers, M.; Szardenings, K.; Lebedev, A.; Gangadharmath, U.; Kolb, H.; Walsh, J.; Zhang, Wiei, Kopka, K.; Wagner, S. Inverse 1,2,3-triazole-1-yl-ethyl substituted hydroxamates as highly potent matrix metalloproteinase inhibitors: (radio)synthesis, in vitro and first in vivo evaluation. *J. Med. Chem.* **2013**, *56* (17), 6858–6870.

(40) Yun, J. I.; Kim, H. R.; Kim, S. K.; Kim, D.; Lee, J. Cross-Metathesis of allyl halides with olefins bearing amide and ester groups. *Tetrahedron* **2012**, *68* (4), 1177–1184.

(41) Shibatomi, K.; Kitahara, K.; Sasaki, N.; Kawasaki, Y.; Fujisawa, I.; Iwasa, S. Enantioselective decarboxylative chlorination of β-ketocarboxylic acids. *Nat. Commun.* **2017**, *8*, 1–7.

(42) Wittig, C.; Schepmann, D.; Soeberdt, M.; Daniliuc, C. G.; Wünsch, B.

Stereoselective synthesis of conformationally restricted KOR agonists based on the 2,5-diazabicyclo[2.2.2]octane scaffold. *Org. Biomol. Chem.* **2017**, *15* (31), 6520–6540.

(43) Geiger, C.; Zelenka, C.; Lehmkuhl, K.; Schepmann, D.; Englberger, W.; W€ Unsch, B. Conformationally constrained K receptor agonists: stereoselective synthesis and pharmacological evaluation of 6,8-diazabicyclo[3.2.2]nonane derivatives. *J. Med. Chem* **2010**, *53*, 4212–4222.

(44) Kracht, D.; Rack, E.; Schepmann, D.; Fröhlich, R.; Wünsch, B. Stereoselective synthesis and structure–affinity relationships of bicyclic κ receptor agonists. *Org. Biomol. Chem*. **2010**, *8*, 212-225.

(45) Costa, B. R. De; Bowen, W. D.; Hellewell, S. B.; George, C.; Rothman, R. B.; Reid, A. A.; Walker, J. M.; Jacobson, A. E.; Rice, K. C. Alterations in the stereochemistry of the kappa-selective opioid agonist U50,488 result in high-affinity sigma ligands. *J. Med. Chem.* **1889**, *32*, 1996–2002.

(46) Radesca, L.; Bowen, W. D.; Di Paolo, L.; de Costa, B. R. Synthesis and receptor binding of enantiomeric N-substituted cis-N-[2-(3,4-dichlorophenyl)ethyl]-2-(1-pyrrolidinyl)cyclohexylamines as high-affinity sigma receptor ligands. *J. Med. Chem.* **1991**, *34* (10), 3058–3065.

(47) Besnard, J.; Ruda, G. F.; Setola, V.; Abecassis, K.; Rodriguiz, R. M.; Huang, X.-P.; Norval, S.; Sassano, M. F.; Shin, A. I.; Webster, L. A.; Simeons, F. R.; Stojanovski, L.; Prat, A., Seidah, N. G.; Constam, D. B.; Bickerton, G. R.; Read, K. D.; Wetsel, W. C.; Gilbert, I. H.; Roth, B. L.;Hopkins, A. L.Automated design of ligands to polypharmacological profiles. *Nature* **2012**, *492*, 215-220.

(48) Zhang, Y.; Liu, C.; Wei, B.; Pei, G. Loss of β-Arrestin 2 exacerbates experimental

autoimmune encephalomyelitis with reduced number of foxp3 $^{+}$ CD4 $^{+}$ regulatory T cells. *Immunology* **2013**, *140* (4), 430–440.

(49) Veremeyko, T.; Yung, A. W. Y.; Dukhinova, M.; Kuznetsova, I. S.; Pomytkin, I.; Lyundup, A.; Strekalova, T.; Barteneva, N. S.; Ponomarev, E. D. Cyclic AMP pathway suppress autoimmune neuroinflammation by inhibiting functions of encephalitogenic CD4 T cells and enhancing M2 macrophage polarization at the site of inflammation. *Front. Immunol.* **2018**, *9*, 50.

(50) Cheng, Y.; Sun, L.; Xie, Z.; Fan, X.; Cao, Q.; Han, J.; Zhu, J.; Jin, T. Diversity of immune cell types in multiple sclerosis and its animal model: pathological and therapeutic implications. *J. Neurosci. Res.* **2017**, *95* (10), 1973–1983.

(51) Mykicki, N.; Herrmann, A. M.; Schwab, N.; Deenen, R.; Sparwasser, T.; Limmer, A.; Wachsmuth, L.; Klotz, L.; Köhrer, K.; Faber, C.; Wiendl, H.; Luger, T.A.; Meuth, S.G.; Loser, K. Melanocortin-1 receptor activation is neuroprotective in mouse models of neuroinflammatory disease. *Sci. Transl. Med.* **2016**, *8* (362), 362ra146.

(52) Kaskow, B. J.; Baecher-Allan, C. Effector T cells in multiple sclerosis. *Cold Spring Harb. Perspect. Med.* **2018**, *8* (4), a029025.

(53) Rangachari, M.; Kuchroo, V. K. Using EAE to better understand principles of immune function and autoimmune pathology. *J. Autoimmun.* **2013**, *45*, 31–39.

(54) Awasthi, A.; Rangachari, M.; Kleinewietfeld, M.; Sonar, S. A.; Lal, G. Differentiation and transmigration of CD4 T cells in neuroinflammation and autoimmunity. **2017**, *8*, 29.

(55) Börner, C.; Kraus, J. Inhibition of NF-κB by opioids in T cells. *J. Immunol.* **2013**, *191* (9), 4640–4647.

(56) Liang, X.; Liu, R.; Chen, C.; Ji, F.; Li, T. Opioid system modulates the immune function: a review. *Transl. Perioper. pain Med.* **2016**, *1* (1), 5–13.

(57) Kirst, A.; Wack, C.; Lutz, W. K.; Eggert, A.; Kämpgen, E.; Fischer, W. H. Expression of functional κ-opioid receptors on murine dendritic cells. *Immunol. Lett.* **2002**, *84* (1), 41–48.

(58) Domogalla, M. P.; Rostan, P. V.; Raker, V. K.; Steinbrink, K. Tolerance through education: How tolerogenic dendritic cells shape immunity. *Front. Immunol.* **2017**, *8*, 1764.

(59) Carreño, L. J.; Riedel, C. A.; Kalergis, A. M. Induction of tolerogenic Dendritic Cells by NF-κBBblockade and Fcγ Receptor Modulation; Humana Press, Totowa, NJ, 2010; pp 339–353.

(60) García-González, P.; Ubilla-Olguín, G.; Catalán, D.; Schinnerling, K.; Aguillón, J. C. Tolerogenic dendritic cells for reprogramming of lymphocyte responses in autoimmune diseases. *Autoimmun. Rev.* **2016**, *15* (11), 1071–1080.

(61) Hu, S.; Sheng, W. S.; Rock, R. B. Immunomodulatory properties of kappa opioids and synthetic cannabinoids in HIV-1 neuropathogenesis. *J. Neuroimmune Pharmacol.* **2011**, *6* (4), 528–539.

(62) Westman, E.; Thi Ngoc, D. D.; Klareskog, L.; Harris, H. E. Suppressive effects of a quinoxaline-analogue (Rob 803) on pathogenic immune mechanisms in collagen-induced arthritis. *Clin. Exp. Immunol.* **2008**, *152* (1), 192–199.

(63) Maroni, D.; Rana, S.; Mukhopadhyay, C.; Natarajan, A.; Naramura, M. A quinoxaline urea analog uncouples inflammatory and pro-survival functions of IKKβ. *Immunol. Lett.* **2015**, *168* (2), 319–324.

(64) DeHaven-Hudkins, D. L.; Fleissner, L. C.; Ford-Rice, F. Y. Characterization of the

binding of [^{3}H](+)-pentazocine to sigma recognition sites in guinea pig brain. *Eur. J. Pharmacol.* **1992**, *227* (4), 371–378.

(65) Mach, R. H.; Smith, C. R.; Childers, S. R. Ibogaine possesses a selective affinity for sigma 2 receptors. *Life Sci.* **1995**, *57* (4), PL57-62.

(66) Che, T.; Majumdar, S.; Zaidi, S. A.; Ondachi, P.; McCorvy, J. D.; Wang, S.; Mosier, P. D.; Uprety, R.; Vardy, E.; Krumm, B. E.; Han, G.W.; Lee, M.Y.; Pardon, E.; Steyaert, J.; Huang, X.P.; Strachan, R.T.; Tribo, A.R.; Pasternak, G.W.; Carroll, F.I.; Stevens, R.C.; Cherezov, V.; Katritch, V.; Wacker, D.; Roth, B.L. Structure of the nanobody-stabilized active state of the kappa opioid receptor. *Cell* **2018**, *172*, 1–13.

(67) Kroeze, W. K.; Sassano, M. F.; Huang, X.-P.; Lansu, K.; McCorvy, J. D.; Giguère, P. M.; Sciaky, N.; Roth, B. L. PRESTO-Tango as an open-source resource for interrogation of the druggable human GPCRome. *Nat. Struct. Mol. Biol.* **2015**, *22* (5), 362–369.

(68) Liu, W.; Wacker, D.; Gati, C.; Han, G. W.; James, D.; Wang, D.; Nelson, G.; Weierstall, U.; Katritch, V.; Barty, A.; Zatsepin, N.A.; Li, D.; Messerschmidt, M.; Boutet, S.;Williams, G.J.; Koglin, J.E.; Seibert, M.M.; Wang, C.;Shah, S.T.A.; Basu, S.; Fromme, R.; Kupitz, C.; Rendek, K.N.; Grotjohann, I.; Fromme, P.;Kirian, R.A.; Beyerlein, K.R.; White, T.A.; Chapmann, H.N.; Caffrey, M.; Spence, J.C.H.; Stevens, R.C.; Cherezov, V. Serial femtosecond crystallography of G protein-coupled receptors. *Science (80-.).* **2013**, *342* (6165), 1521–1524.

(69) Mykicki, N.; Klenner, L.; Baumann, C.; Auriemma, M.; Sternemann, C.; Soeberdt, M.; Elliott, G. R.; Abels, C.; Luger, T. A.; Loser, K. The tripeptide KdPT ameliorates ongoing psoriasis-like skin inflammation in murine and human skin.

Exp. Dermatol. **2017**, *26* (4), 328–334.

(70) Bittner, S.; Ruck, T.; Schuhmann, M. K.; Herrmann, A. M.; Maati, H. M. ou; Bobak, N.; Göbel, K.; Langhauser, F.; Stegner, D.; Ehling, P.; Borsotto, M.; Pape, H.C.; Nieswandt, B.; Kleinschnitz, C.; Heurteaux, C.; Galla, H.J.; Budde, T.; Wiendl, H.; Meuth, S.G. Endothelial TWIK-related potassium channel-1 (TREK1) regulates immune-cell trafficking into the CNS. *Nat. Med.* **2013**, *19* (9), 1161–1165.

Table of Contents Graphics

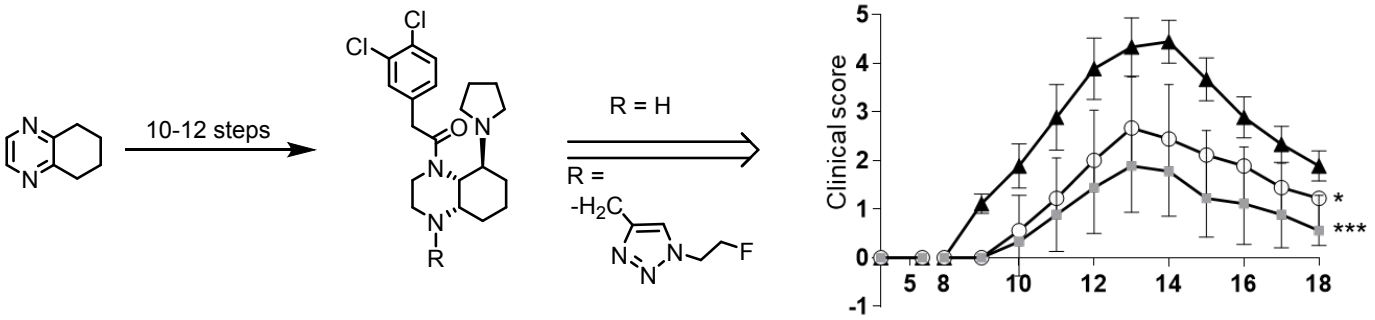

- High affinity and selectivity towards KOR
- Full agonist
- Activation of G protein and β-arrrestin-2

- *in vitro:* anti-inflammatory and immunomodulatory activity in primary mouse and human immune cells
- *in vivo:* beneficial effect in EAE